Cell

Article

Microbiome mismatches from microbiota transplants lead to persistent off-target metabolic and immunomodulatory effects

Graphical abstract

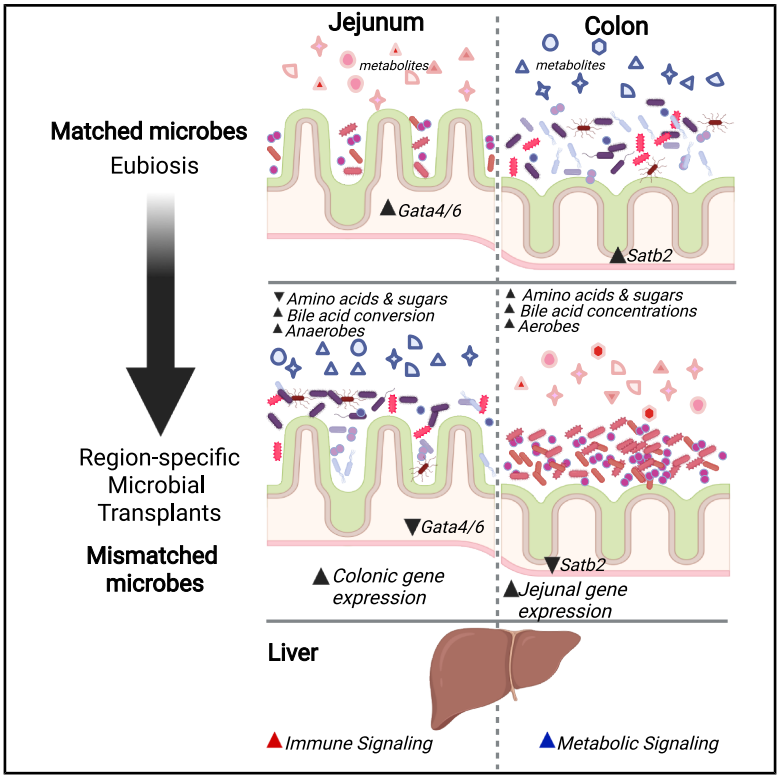

Authors

Orlando DeLeon, Mora Mocanu, Alan Tan, ..., David T. Rubin, Kristina Martinez-Guryn, Eugene B. Chang

Correspondence

kmarti2@midwestern.edu (K.M.-G.), echang@bsd.uchicago.edu (E.B.C.)

In brief

Fecal microbiota transplants (FMTs) may not always effectively restore small bowel microbiota due to regional differences in gut environments, potentially causing unintended effects on metabolism and immune function. This research suggests that personalized, intestinal-region-specific microbiome therapies are needed to improve outcomes and avoid mismatches that could impact gut health and disease.

Highlights

- Microbes alter regional intestinal environments to enhance fitness and engraftment
- Mismatches alter metabolic and immune states of host tissues and regional microbiomes
- Engraftment of FMT (anaerobic) microbes in the small bowel is persistent
- Regionally matched microbiota in the small and large bowel restore homeostasis

DeLeon et al., 2025, Cell *188*, 3927–3941
July 24, 2025
https://doi.org/10.1016/j.cell.2025.05.014

CellPress

Cell

CellPress

Article

Microbiome mismatches from microbiota transplants lead to persistent off-target metabolic and immunomodulatory effects

Orlando DeLeon,[1,8] Mora Mocanu,[1,8] Alan Tan,[1] Ashley M. Sidebottom,[2] Jason Koval,[1] Hugo D. Ceccato,[1] Sarah Kralicek,[3] John J. Colgan,[1] Marissa M. St. George,[1] Joash M. Lake,[1] Michael Cooper,[1] Jingwen Xu,[1] Julia Moore,[3] Qi Su,[4,5,6] Zhilu Xu,[4,5,6] Siew C. Ng,[4,5,6,7] Francis K.L. Chan,[4,5,6] Hein M. Tun,[4,5,6] Candace M. Cham,[1] Cambrian Y. Liu,[1] David T. Rubin,[1] Kristina Martinez-Guryn,[3,*] and Eugene B. Chang[1,9,*]

[1]Department of Medicine, University of Chicago, Chicago, IL 60637, USA
[2]Duchossois Family Institute, University of Chicago, Chicago, IL 60637, USA
[3]Department of Biomedical Science, Midwestern University, Downers Grove, IL 60515, USA
[4]Department of Medicine and Therapeutics, The Chinese University of Hong Kong, Hong Kong SAR, China
[5]Microbiota I-Center (MagIC), Hong Kong SAR, China
[6]Li Ka Shing Institute of Health Sciences, State Key Laboratory of Digestive Disease, Institute of Digestive Disease, The Chinese University of Hong Kong, Hong Kong SAR, China
[7]New Cornerstone Science Laboratory, The Chinese University of Hong Kong, Hong Kong SAR, China
[8]These authors contributed equally
[9]Lead contact
*Correspondence: kmarti2@midwestern.edu (K.M.-G.), echang@bsd.uchicago.edu (E.B.C.)
https://doi.org/10.1016/j.cell.2025.05.014

SUMMARY

Fecal microbiota transplant (FMT) is an increasingly used intervention, but its suitability to restore regional gut microbiota, particularly in the small bowel (SB), must be questioned because of its predominant anaerobic composition. In human subjects receiving FMT by upper endoscopy, duodenal engraftment of anaerobes was observed after 4 weeks. We hypothesized that peroral FMTs create host-microbe mismatches that impact SB homeostasis. To test this, antibiotic-treated specific-pathogen-free (SPF) mice were given jejunal, cecal, or fecal microbiota transplants (JMTs, CMTs, or FMTs, respectively) and studied 1 or 3 months later. JMT and FMT altered regional microbiota membership and function, energy balance, and intestinal and hepatic transcriptomes; JMT favored host metabolic pathways and FMT favored immune pathways. MTs drove regional intestinal identity (*Gata4*, *Gata6*, and *Satb2*) and downstream differentiation markers. RNA sequencing (RNA-seq) of metabolite-exposed human enteroids and duodenal biopsies post-FMT confirmed transcriptional changes in mice. Thus, regional microbial mismatches after FMTs can lead to unintended consequences and require rethinking of microbiome-based interventions.

INTRODUCTION

Fecal microbiota transplant (FMT) is an increasingly used intervention to promote repair of intestinal dysbiosis.[1–3] Although FMT is effective for recurrent *Clostridioides difficile* infection, its mechanisms, efficacy, and off-target consequences in other disorders, including obesity, autism, cancer, and inflammatory bowel diseases, remain unclear.[4–10] Anecdotal reports have included gastrointestinal (GI) distress, sepsis, and metabolic consequences, including an adult female who experienced weight gain after receiving an FMT[11–13] as well as a flare of ulcerative colitis.[14]

Often overlooked is that regional gut microbiota differ in membership and function, matching their ecosystem to remain fit and benefit the host.[15,16] Small bowel microbiota (SBM) confer a functional impact on the host distinct from colonic microbiota. For example, a Western-style high-fat, low-fiber diet profoundly alters jejunal microbiota composition to directly influence lipid digestion and absorption.[17,18] SBM have also been shown to regulate hepatic and central (nervous system) circadian clock genes, cortical microglia, intestinal nutrient processing, and energy balance.[18–23] Regional ecosystems of the gut are distinct and confer selective environmental features, gene expression, cells, and functions that selects for microbial colonization.[24–26] The small bowel (SB) is the site of macronutrient digestion and absorption, with greater levels of pancreatic enzymes, bile, and intestinal villi coated in a thin mucus layer.[27] By contrast, the large bowel (LB) is largely anaerobic, contains significant levels of short-chain fatty acids (SCFAs) and non-digestible plant polysaccharides, thick mucus, and is the major site for primary to

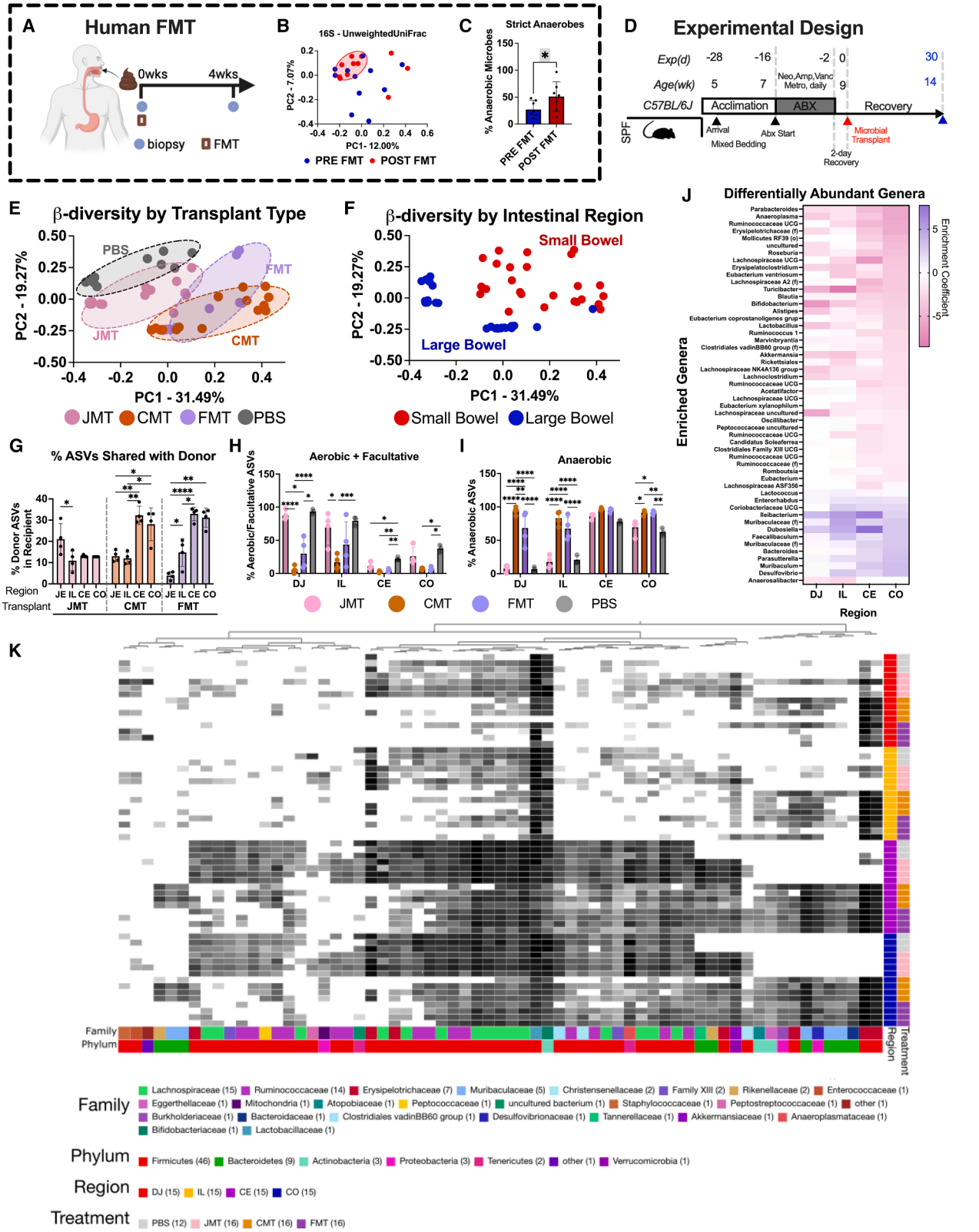

(legend on next page)

secondary bile acid (BA) conversion, water reabsorption and stool formation.[28] These characteristics are driven by central regulators, including GATA binding protein 4 and 6 (*Gata4/Gata6*) in the jejunum and special AT-rich sequence binding protein 2 (*Satb2*) in the colon, that control downstream expression of differentiation markers associated with the respective tissues.[29–32] Considering that large bowel microbiota (LBM) are predominantly anaerobic and differ in composition and function to SBM, the appropriateness of FMT to reconstitute the SB must be questioned as they are composed of non-indigenous and likely unfit microbes.

Colonization of the SB by anaerobes in FMT patients has been associated with changes to weight.[33] We confirmed this report of anaerobic colonization in the SB by 16S rRNA assessment of duodenal biopsies after FMT. Considering the importance of the SBM in metabolism,[15,16] we hypothesized that anaerobic colonization of the SB after FMT drives microbe-to-regional ecosystem mismatches and effects metabolic consequences in the host.

RESULTS

SB and LB MTs colonize the gut and shift native, regional microbial communities

We examined $n = 7$ subjects receiving FMT from an upper endoscopy and performed 16S rRNA amplicon sequencing on samples before FMT and after 1 month (Figure 1A). Although no significant difference was found in the β-diversity (Figure 1B; unweighted UniFrac, PERMANOVA, p = NS), we measured an increase in strict anaerobes after FMT (Figure 1C; Student's paired t test, $^*p < 0.05$) confirming the report of significantly increased anaerobic colonization in the SB.[33]

Due to the differences between SBM and LBM, we hypothesized that anaerobic colonization of the SB would have adverse consequences in the host. As this is difficult to study in humans, we utilized a post-antibiotic model of different microbiota transplantation (MT) to better characterize the consequences of regional microbiota mismatch.[34–38] C57Bl6 mice from Jackson Labs (JAX) were treated with a 2-week course of antibiotics (ABX; ampicillin, vancomycin, neomycin, and metronidazole), after which they were given a single SBM transplant (jejunal and JMT [jejunal microbiota transplant]), an LBM transplant (colonic and FMT), a mixture of SBM and LBM transplants (cecal and CMT [cecal microbiota transplant]), or no MT (phosphate buffered saline [PBS]) from in-house-bred donors and delivered by oral gavage (Figure 1D). CMT and FMT inoculum were diluted 1:10 to accommodate higher CFUs in the LB. First, we examined the microbiota within each regional intestinal ecosystem through 16S rRNA sequencing to determine whether MTs altered composition. Luminal contents were taken directly from each intestinal region at the time of sacrifice and thus represent the microbiota communities specific to the LB and SB. Comparison of β-diversity across the intestinal tract (Figures 1E and 1F) demonstrated separation by both MT and region (SB vs. LB), suggesting that differences in the microbiota and the ecosystem they encounter determine regional microbiota composition (unweighted UniFrac, PERMANOVA, $p < 0.05$, all pairwise comparisons). Examination of each intestinal region demonstrated unique microbial compositions within each intestinal compartment (Figures S1A–S1D) and MT-dependent changes to α diversity (Figures S1E–S1H).

Next, we assessed engraftment of the transplanted microbes by calculating the percentage of amplicon sequence variants (ASVs) specific to each MT. It is well known that microbiota differ drastically between animal facilities, each mouse colony harboring distinct microbial strains. Assessment of ASV overlap revealed ≤5% were common between Jackson Labs (JAX) and our facility.[39] Unambiguous donor strains comprised 5%–35% of the ASVs in the resulting microbiota communities (Figure 1G). Unsurprisingly, JMT microbes colonized the jejunum (20%), with lower efficiencies in the cecum and colon (15%). FMTs and CMTs colonized the anaerobic environments of the cecum and colon best at 28%–30%, with lower engraftment in the aerobic jejunum (5%–10%). This corresponded to higher levels of aerobes after JMT and anaerobes following FMT (Figures 1H and 1I). These included the aerobic genus *Lactobacillus* in JMT mice and anaerobic *Ileibacterium*, *Dubosiella*, *Faecalibaculum*, *Enterorhabdus*, and *Desulfovibrio* in FMT mice (Figure 1J). Entire bacterial families appeared absent within given intestinal regions, demonstrating the large effect of MT on restoring (or not restoring) the regional microbiota (Figure 1K). The number of unique, non-redundant ASVs from donor transplant material detected in recipient animals was determined. A total of 449 non-redundant ASVs were identified

Figure 1. Small and large bowel MTs colonize the gut and shift native regional microbial communities

(A) Sample collection in human FMTs.

(B) 16S rRNA sequencing of intestinal contents 1 month post MT. Principal coordinate analysis (PCoA) of the β diversity by unweighted UniFrac distances (pre-FMT, blue; post-FMT, red; PERMANOVA, not significant; $p > 0.05$).

(C) Percentage of strict anaerobes before and after FMT (Student's t test, $^*p < 0.05$).

(D) Experimental design of post-antibiotic transplant model in mice.

(E and F) 16S rRNA sequencing of intestinal contents 1 month post MT. Principal coordinate analysis (PCoA) of the β diversity by unweighted UniFrac distances of all samples colored by MT type (E) (phosphate buffered saline [PBS], gray; JMT, pink; CMT, orange; FMT, lavender) and by intestinal regions (F) (small bowel, red; large bowel, blue; PERMANOVA, $^*p < 0.001$).

(G) Percentage of ASVs that originated from donor (MT engraftment) for each type of transplant in the jejunum, ileum, cecum, and colon (ANOVA, $^*p < 0.05$).

(H and I) Percentage of aerobic and facultative microbes and anaerobic microbes by 16S rRNA sequencing, respectively (ANOVA, post hoc Tukey's, $^*p < 0.05$).

(J) Differentially abundant genera between JMT and FMT in each intestinal region. Maaslin2-generated significant enrichment coefficients are shown for JMT-enriched (pink) and FMT-enriched (lavender) genera.

(K) Heatmap of top 50 genera ($\log_2$ scale) across treatments and gut regions.

Abbreviations in this figure include DJ, duodenum-jejunum; JE, jejunum; IL, ileum; CE, cecum; and CO, colon. All error bars indicate ± SD.

Related to Figures S1, S2, and S3.

in the donor transplant material. 109 ASVs were detected in the JMT donor materials, 217 in the FMT, and 422 ASVs in the CMT donor materials across all experiments. Of these ASVs, an average of 18.27 (*SD* = ±10.64) were detected in JMT-recipient mice, 34.42 (*SD* = ±18.12) were detected in CMT-recipient mice, and 27.97 (*SD* = ±14.32) were detected in the FMT-recipient mice. ASV-specific engraftment in each region is detailed in Figure S2, with an average of 10%–30% of donor ASVs engrafting within the recipient mice (Figures S2B and S2C). Engraftment and MT-specific differences in composition were observed up to 3 months, underscoring the persistent engraftment of the single transplant (see Data S1). To assay changes to the functional potential of the resulting microbiota communities after MT, we performed shotgun metagenomic sequencing on the colonic contents of these animals and performed KEGG Orthology (KO) pathway analysis, comparing those enriched in a given transplant over the PBS control (Figure S3). Pathway analysis demonstrated a recovery of more pathways after CMT and FMT (95 and 79, respectively) than JMT (45), with many of these pathways shared across all transplants but specific to others (Figures S3B and S3C). Interestingly, JMT metagenomes were particularly enriched for fatty acid biosynthesis pathways and lower in beta-oxidation genes, bile salt hydrolases, and 7α-HSDHs (Figures S3D–S3K; ANOVA, $^*p < 0.05$).

Together, these data demonstrate that a single MT of SBM and LBM can successfully engraft the entirety of the intestinal tract (not only their native niche), that it can change the regional microbial composition and functional potential, and that this colonization is persistent. This extends the parallel observations of increased and persistent anaerobic colonization of the SB after FMT in humans.

SB and LB MTs alter regional and systemic metabolite pools

Regional differences extend to metabolite concentrations, driven in part by geographically specific microbial transformations.[40] These metabolites can act as signaling molecules to affect host health.[41–43] To characterize the functional output of the microbiome, we performed targeted metabolomics on duodenum-jejunum and colon luminal contents.

We assayed 300+ known human and microbially produced or modified compounds, ranging from BAs, SCFAs, and amino acids to carbohydrates/sugars. 70 compounds were differentially abundant between JMT and FMT in either the duodenum-jejunum or colon (Figures 2A and 2B, respectively; ANOVA, *p*adj < 0.05 shown). Differences between JMT and FMT regional metabolomes were visualized with principal-component analysis (PCA), highlighting the impact of MT type on the microbiome functional output (Figures 2C–2E; PERMANOVA, $p < 0.05$ for JMT vs. FMT). PBS and FMT displayed similar metabolomic profiles. In the FMT duodenum-jejunum, we detected higher levels of propionate; lower levels of complex carbohydrates such as cellobiose and simple sugars such as sucrose, glucose, and fructose; and lower sugar alcohols such as mannitol, maltitol, sorbitol, and dulcitol. In the FMT colon, we detected lower levels of sugars/sugar alcohols and amino acids, including leucine, isoleucine, tyrosine, methionine, valine, phenylalanine, asparagine, and lysine, compared with JMT. Large differences were observed in the BA pool, including lower conjugated BAs like tauro-chenodeoxycholic acid (tauroCDCA), taurocholic acid (tauroCA), and glycocholic acid (glycoCA). We found that JMT increased the total concentration of BAs in the duodenum-jejunum (Figure 2F; ANOVA, $p < 0.05$), decreased the percentage of secondary BAs in the colon (Figure 2G; ANOVA, $p < 0.05$), and had a trending but not significant increase in the conjugated BA ratio (Figure 2H; ANOVA, $p > 0.05$).

We found MTs also affected systemic circulating metabolite pools in plasma, with distinct differences between JMT and FMT visualized by both PCA and heatmap (Figures 2J and 2I; PERMANOVA, JMT vs. FMT, $p < 0.05$). Plasma carbohydrates and amino acids aspartic acid, glutamic acid, and proline were enriched in JMTs, whereas isoleucine was enriched in FMTs (Figure 2I; ANOVA, $p < 0.05$). However, the circulating fatty acids palmitic acid, myristic acid, linoleic acid, and *cis*-oleic acid were found to be circulating at higher concentrations in FMT vs. JMT. This correlated to shifts in the circulating BA pools (Figures 2K–2M). Plasma total BA concentrations were significantly increased in the JMT-treated animals (ANOVA, $p < 0.05$), with increased conjugated BAs detected. These differences were driven by enrichments of beta-muricholic acid and CA in JMT mice, with persistent changes to the metabolome up to 3 months characterized by similar changes to amino acids, BAs, and carbohydrate concentrations (see Data S1). Together, these data indicate that SBM and LBM affect both composition and functional output of regional gut microbiota, impacting many classes of microbially modified and produced metabolites.

GF mice reflect similarities to the ABX model

The coprophagic nature of mice can complicate interpretation of FMT studies through repeat inoculation of fecal microbiota.[44] Additionally, treatment with antibiotics and native microbiota can affect donor engraftment (despite a 2-day period prior to transplant to allow for antibiotic clearance). To understand how SBM and LBM colonize in the absence of competition, antibiotic effects, and self-inoculation (via coprophagy) with fecal microbiota, we transplanted JMT and FMT in germ-free (GF) mice (which can only re-inoculate themselves with the transplanted microbiota) and performed 16S rRNA amplicon sequencing and metabolomics.

Similar to our post-antibiotic mouse model, we found that transplant type and intestinal region affected microbiota composition (Figures 3A and 3B; unweighted UniFrac, PERMANOVA, $p = 0.001^*$). With the exception of the ileum, each intestinal compartment had distinct communities (Figures S4A–S4E; unweighted UniFrac, PERMANOVA, $p = 0.001^*$). Despite the absence of competing microbes, FMT did not colonize the SB as efficiently as the LB, (∼20% more) (Figure 3C). Although JMT microbes colonized the SB more efficiently than FMT microbes (∼40%), JMT colonization of the LB varied (20%–90%). SB aerobic and facultative colonization increased following JMT, with anaerobic colonization increased after FMT (Figures 3D and 3E, respectively). However, no difference was found in the LB. Interestingly, JMT-SPF (specific-pathogen-free) mice displayed higher levels of aerobes and lower levels of anaerobes in the SB when compared with JMT-GF mice, which may be due to the high variability of oxygen in the SB of GF mice (Figures 3F and 3G).[45] Differentially

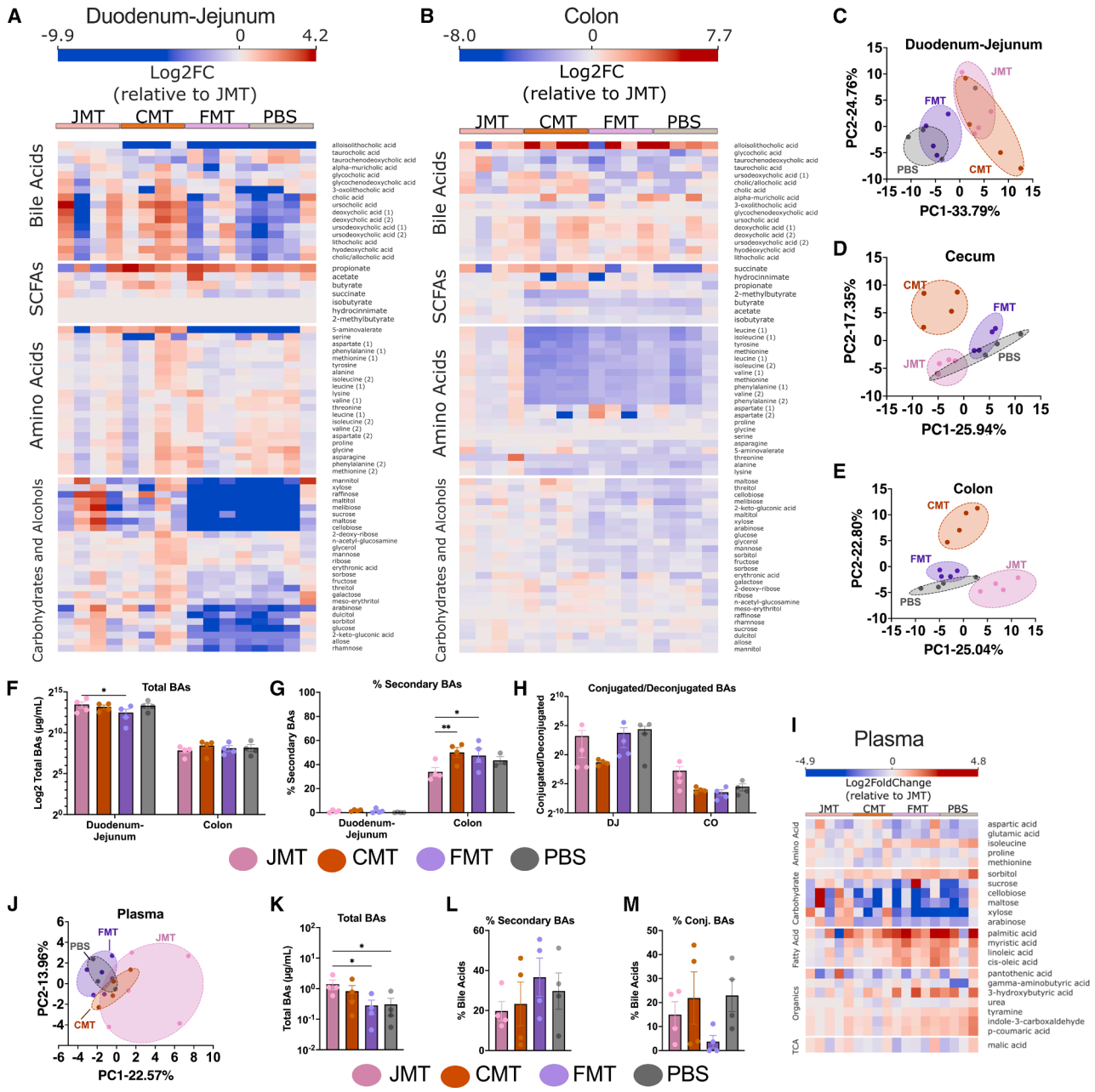

Figure 2. Small and large bowel MTs alter regional and systemic metabolite pools

(A and B) Heatmap of differentially abundant metabolites within the duodenum-jejunum and colon from targeted metabolomics. Values are expressed in $\log_2$ fold change relative to the average abundance in JMT (red > JMT, blue < JMT) for any metabolite with a significant change between any pairwise comparison (ANOVA, post hoc Tukey's, $^*p < 0.05$).

(C–E) Principal-component analysis (PCA) of the $\log_2$ normalized metabolite abundances in the duodenum-jejunum, cecum, and colon (JMT, pink; CMT, orange; FMT, lavender; PBS, gray).

(F–H) Targeted metabolomics and absolute quantification of the 16 most abundant bile acids detected in the duodenum-jejunum and colon represented as total bile acids, percentage of secondary bile acids, and conjugated/deconjugated bile acids (ANOVA, post hoc Tukey's, $^*p < 0.05$).

(I) Heatmap of differentially abundant metabolites within plasma. Values are expressed in $\log_2$ fold change relative to the average abundance in JMT (red, enriched; blue, depleted) for any metabolite with a significant change between any pairwise comparison (ANOVA, post hoc Tukey, $^*p < 0.05$).

(J) PCA of metabolites found in plasma (PERMANOVA, Mann-Whitney,$^*p < 0.05$ for JMT vs. FMT).

(K–M) Targeted metabolomics and absolute quantification of the top 16 bile acids detected in plasma represented as total bile acids, percentage of secondary bile acids, and percentage of conjugated bile acids (ANOVA, post hoc Tukey's, $^*p < 0.05$). All error bars indicate ± SE.

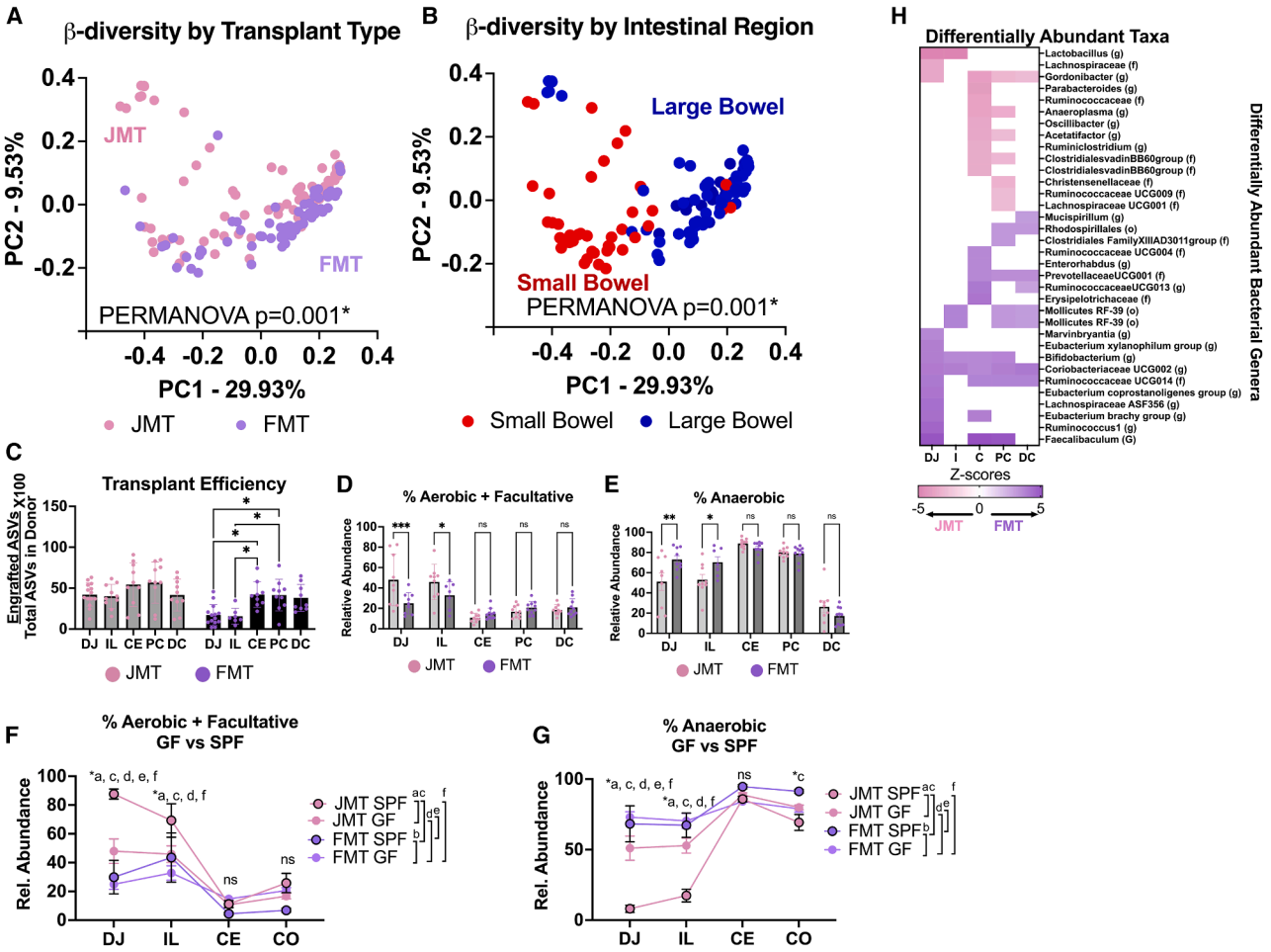

Figure 3. GF mice reflect similarities to the ABX model

(A and B) 16S rRNA sequencing of intestinal contents 1 month post MT. Principal coordinate analysis (PCoA) of the β diversity by unweighted UniDFrac distances of all samples colored by MT type (A) (JMT, pink; FMT, lavender) and by intestinal regions (B) (small bowel, red; large bowel, blue; PERMANOVA, $^*p < 0.001$ for all JMT vs. FMT and SB vs. LB).

(C) MT transfer efficiency, calculated as the percent of the total no. of ASVs from the MT/total no. of ASVs in the MT (one-way ANOVA, post hoc Tukey's, $^*p < 0.05$ for duodenum-jejunum and ileum relative to the cecum and proximal colon for FMT).

(D) Percentage of aerobic + facultative microbes are higher for JMT in the SB (ANOVA, post hoc Tukey's, $^*p < 0.05$).

(E) Percentage of anaerobic microbes are higher in the SB after FMT (ANOVA, post hoc Tukey's, $^*p < 0.05$).

(F and G) Comparison of SPF and GF abundances of aerobic+ facultative or anaerobic microbes (ANOVA, post hoc Tukey's, $^*p < 0.05$).

(H) Linear discriminant analysis effect size (LEfSe) to detect differentially abundant microbes in each region.

Abbreviations in this figure include DJ, duodenum-jejunum; JE, jejunum; IL, ileum; CE, cecum; CO, colon; PC, proximal colon; and DC, distal colon. All error bars indicate ± SD.

Related to Figure S4.

enriched microbes were similar to the SPF mice, including JMT-enriched aerobic *Lactobacillus* and FMT-enriched *Rumminococcaceae*, *Eubacterium*, *Coriobacteriaceae*, *Faecalibaculum*, and *Enterorhabdus* (Figure 3H; *MaAsLin2*, $p < 0.05$). These correlated to metabolite profiles found in SPF animals, including JMT-enriched intestinal amino acids, decreased SCFAs, increased total BAs in the duodenum-jejunum and colon, increased conjugated BAs in the colon, and reduced secondary BAs (Figures S4F–S4I; Data S1). Together, these data show that without the complications of antibiotics, native microbiota competition, and re-inoculation with fecal microbiota, GF mice display similar patterns of colonization and metabolite profiles across the gut, including anaerobic colonization of the SB. Additionally, GF mice exhibit altered regional and systemic BAs pools consistent with our post-antibiotic mice and the "fecal collection" cup models known to prevent coprophagy, including increased total and reduced secondary BAs.[44,46–48]

MTs drive divergent hepatic transcriptional programs that persist for up to 3 months and shift energy balance

Many BAs, carbohydrates, and amino acids are bioactive and have large effects on metabolism as signaling molecules and in

total nutrient flux. Metabolites from the gut are absorbed throughout the intestinal tract, collected by the intestinal vascular system, and enter the liver via the hepatic portal vein. The liver is a major metabolic organ of the body and the first organ outside of the gut to encounter microbial products. Given the changes in intestinal colonization, metabolite pools, and the role of SBM in metabolism, we asked how regional microbial mismatches affected distant organs like the liver.

We performed RNA sequencing (RNA-seq) to examine hepatic transcriptional profiles after MT. Hepatic transcriptomes of each MT group were unique, with the largest differences observed between JMT and FMT recipients (PC1–16.57%) and with CMT recipients displaying an intermediate phenotype (PERMANOVA, $p < 0.05$ for all pairwise comparisons) (Figure 4A). Differential gene expression analysis confirmed the largest differences between JMT and FMT, with 3,928 differentially expressed genes (DEGs) (Figure 4B). 2,504 DEGs were found for JMT vs. CMT and 1,805 DEGs were found for FMT vs. CMT (DESeq2, padj < 0.05) (Figures 4C and 4D). Strikingly, JMT enriched for metabolic- and lipid-associated genes, including ELMO domain containing 3 (*Elmod3*), cytochrome p450s *Cyp4a14 and Cyp4a32*, perilipin 5 (*Plin5*), peroxisomal biogenesis factor 11 alpha (*Pex11a*), solute carrier *Slc25a47*, and acyl-CoA thioesterase (*Acot*)*1/2*. FMT expressed enriched serum amyloid A3 (*Saa3*), lipocalin 2 (*Lcn2*), ephrin A3 (*Efna3*), interleukin 33 (*Il-33*), T-cell receptor-associated transmembrane adapter 1 (*Trat1*), and alpha kinase 1 (*Alpk1*), all involved in immune function. To better understand differences in gene expression, we mapped the profiles onto KEGG Ontology pathways (*fGSEA*, R-package, padj < 0.05). Pathway analysis revealed that 10 out of 14 FMT-enriched KEGG pathways were immune related, including "pathogenic *E. coli* infection," "cytokine-cytokine signaling," "chemokine signaling," "RIG-I like signaling," "TLR signaling," and "NOD-like signaling." Conversely, the top pathways enriched in JMTs were associated with metabolism, including "PPAR-signaling," "oxidative phosphorylation," "fatty acid metabolism," "synthesis of unsaturated fatty acids," "BCAA degradation," and "linoleic acid metabolism" (Figure 4E). Transcriptional changes were detected 3 months post transplant (Figure S5) and observed in GF mice (Figure 4F; Data S1), suggesting the shifts in hepatic transcriptomes are persistent and a direct effect of the microbial transplants.

Due to the impact on metabolic pathways of the liver, we examined the energy balance of these animals using metabolic cages and assessed eating behaviors, activity, energy expenditure, and nutrient utilization (Promethion, Sable Systems). JMT mice weighed the most after 1 month, gained the greatest amount of weight, and displayed the lowest energy expenditure (Figures 4G, 4H, and 4K; ANOVA, $p < 0.05$) and lowest activity (Figure 4J; ANOVA, $p < 0.05$). FMT mice had the lowest food intake of any group but displayed higher levels of energy expenditure relative to JMT mice (Figure 4I; ANOVA, $p < 0.05$). Interestingly, activity, food intake, maintenance of weight and weight change, and energy expenditure suggested CMT mice were the most metabolically active (Figure 4G–4K; ANOVA, $p < 0.05$, for all comparisons vs. CMT). The low respiratory exchange ratio (RER) in CMT mice suggests increased lipid oxidation, congruent with increased energy expenditure and utilization of fats as an energy source (Figure 4L; ANOVA, $p < 0.05$).

Furthermore, we identified potential bacterial strains that may potentiate JMT vs. FMT hepatic transcriptional changes though a cross-omics analysis of bacterial shotgun metagenomic and the liver RNA-seq data (Figure S3L). We reconstructed 87 high-quality metagenome-assembled genomes (MAGs) and performed a functional enrichment analysis to identify differentially abundant MAGs containing enriched functions in either JMT or FMT. Changes in MAG abundances were compared with hepatic transcriptional changes using Sparse Peak Association Relationship Correlation Calculation (SPARCC) and the two analyses plotted on the x and y axes to identify specific bacterial strains associated with upregulation or downregulation of hepatic transcriptomes (Figure S3M). We identified 5 groups of genes that were associated with specific bacterial genomes. For example, group 2 genes, associated with mitochondrial degradation and peroxisome proliferator-activated receptor alpha (PPARA), were negatively associated with FMT-enriched genomes Bacteroides_03 and Muribaculum_02, whereas group 1 genes, related to mitochondrial and respiration pathways, were associated with FMT-specific genomes Desulfovibrio_01 and Bacteroides_02 (see Table S1 for full MAG characteristics and gene associations). Together, these data highlight the dichotomous impact of SBM and LBM on the host when mismatched to the ecosystem, in particular their divergent effects on metabolic and immune regulation, respectively, and the potential benefits of reconstituting both SBM and LBM.

SBM and LBM change non-indigenous regional gut ecosystems to be more conducive for their engraftment and fitness

It is clear that transplantation of native vs. non-native microbes yield drastic changes in microbiota composition and function to affect host metabolism and distal organs (i.e., the liver). Therefore, we thought it important to characterize how regional gut ecosystems respond to the presence of native vs. non-native microbes and performed RNA-seq on the jejunal and colonic mucosa. PCA of the colonic and jejunal transcriptomes revealed 87% variation (PC1), highlighting large differences between gene expression (Figure 5A). Similar to the metabolomic and hepatic profiles, we found that FMT and PBS intestinal profiles were very similar, owing to the repeat inoculation of LB microbes in coprophagic animals. We noted jejunum from FMT mice had a smaller PC1 difference than the colonic samples, suggesting similarity to colonic tissues (~20%). To probe this deeper, we examined the expression of jejunal and colonic marker genes. Jejunum-specific genes were enriched in the jejunal mucosa of JMT-recipient mice over FMT and PBS controls (ANOVA, $p < 0.05$) (Figure 5B). These included *Gata4* and *Gata6* (G-A-T-A binding proteins), which are central transcriptional regulators of jejunal identity[31,32]; lipid binding and transport genes including apolipoproteins *Apoa1*, *Apoa4*, and cluster of differentation 36/fatty acid translocase (*Cd36*/*Fat*)); and sugar transporters/solute carrier family members *Slc2a2*, *Slc2a5*, and *Slc5a1*. JMTs expressed higher levels of most sugar transporters (see Data S1). In the colon, FMTs expressed higher levels of colon-specific genes, including *Satb2* that drives colonic identity; calcium-activated chloride channel regulator 1 (*Clca1*), carbonic anhydrase 1 (*Car1*), lymphocyte antigen 6 family member G (*Ly6g*), and

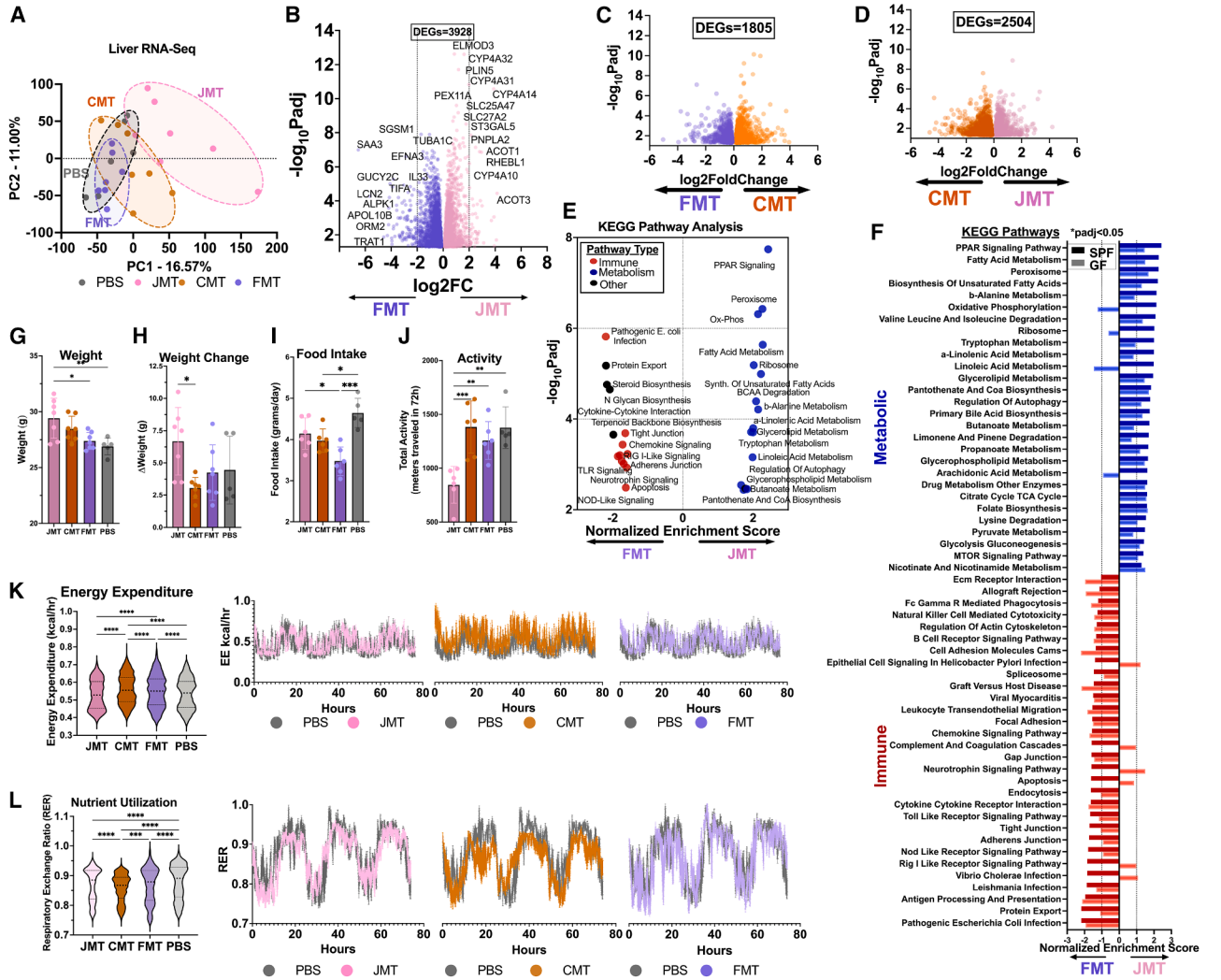

Figure 4. MTs drive divergent hepatic transcriptional programs that persist and shift energy balance

(A) RNA-seq analysis of hepatic tissues 1 month post MT. Relative differences in the hepatic transcriptomes using DESEQ2-analyzed counts and visualized by principal-component analysis colored by MT type. PBS, gray; JMT, pink; CMT, orange; FMT, lavender (PCA, PC1-16.57%, PC2-11%, PERMANOVA, $*p < 0.001$ JMT vs. FMT).

(B–D) Volcano plot of differentially expressed genes between JMT vs. FMT, CMT vs. FMT, and JMT vs. CMT.

(E) Kyoto Encyclopedia of Genes and Genomes (KEGG) pathway analysis of differentially enriched metabolic (blue), immune pathways (red), and other (black) (*fGSEA*, R).

(F) Comparison of GF and SPF differentially enriched pathways.

(G–J) Energy balance assessments using the Sable Systems Promethion Respirometry System demonstrate differences in weight, weight gain, food intake, and activity for JMT vs. FMT mice (ANOVA, $*p < 0.05$).

(K and L) Differences in the energy expenditure and nutrient utilization were observed for all treatment groups relative to PBS (ANOVA, $*p < 0.05$), with traces of 76 h data. All error bars indicate ± SD.

Related to Figures S3 and S5.

desmoglein 2 (*Dsg2*); the colon-specific water transporter aquaporin 8 (*Aqp8*); and SCFA transporters *Slc16a3* and *Slc5a8* (ANOVA, $p < 0.05$) (Figure 5C). Interestingly, antimicrobial peptides typically expressed in the jejunum were enriched after FMT, including defensin alpha 3 (*Defa3*), lysozymes *Lyz1*, *Lyz2*, and matrix metalloproteinase (*Mmp7*), and coincided with changes to Erb-B2 receptor tyrosine kinase 3 (*Erbb3*) and atonal homolog 1 (*Atoh1*), Paneth cell development genes (see Data S1).

These data suggest that mismatched, non-native microbes can re-program the identity of the tissue, enhancing genes conducive to adaptation and engraftment. This would explain the sustained presence of anaerobes in the jejunum 3 months after a single FMT. To quantify the extent to which JMTs and FMTs alter regional ecosystems of the jejunum and colon, we examined RNA-seq data of jejunal and colonic mucosal scrapings derived from healthy, non-ABX-treated C57Bl6 mice and

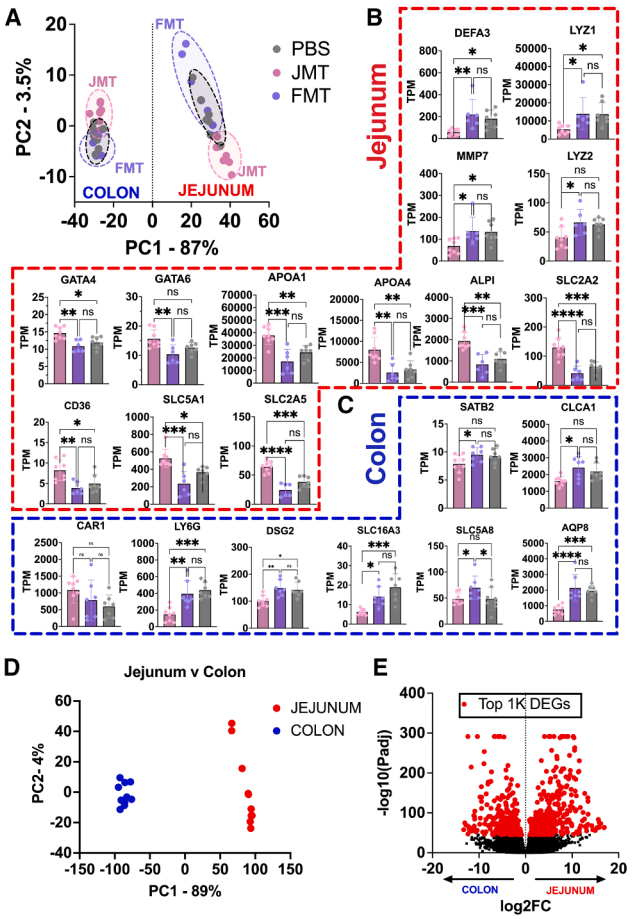

Figure 5. Small and large bowel microbiota condition their regional ecosystems to a more indigenous environment

(A) RNA-seq analysis of intestinal mucosal tissues after 1 month post MT. Principal-component analysis (PCA) of colonic and jejunal tissues demonstrate skewing of FMT jejunal tissues toward colonic samples, JMT, pink; FMT, lavender; and PBS, gray.

(B and C) Expression of jejunal marker genes in the jejunum and colonic marker genes in the colon expressed as transcripts per million (TPM) (ANOVA, post hoc Tukey's, *$p < 0.05$).

(D and E) PCA of jejunal and colonic transcriptomes from healthy, non-ABX-treated C57Bl6, and the top 1,000 differentially expressed genes ($log_2FC > 2$, $padj < 0.05$) were used to generate jejunal and colonic gene sets.

(F) Pathway analysis of jejunal tissues demonstrate an enrichment of the jejunal signature after JMT (NES = 2.48, *padj = 2.75e−22) and an enrichment of the colonic signature in the colon after FMT (NES = 1.54, *padj = 2.84e−3).

(G) Pathway analysis of colonic tissues demonstrate an enrichment of the jejunal signature after JMT (NES = 1.52, *padj = 8.48e−5) and an enrichment of the colonic signature in the colon after FMT (NES = 2.48, *padj = 3.35e−16). All error bars indicate ± SD.

Related to Figure S6.

identified the top 1,000 DEGs (Figures 5D and 5E; $padj < 0.05$, $log_2FC \geq 2$). From these genes, we created "jejunal signature" and "colonic signature" gene sets to performed enrichment analysis of MT intestinal tissues. We found that JMT enriched for jejunal signature (NES = 2.48, padj = 2.75e−22), whereas FMT enhanced the colonic signature (NES = 1.54, padj = 2.83e−3) in the jejunum (Figure 5F). A similar pattern was observed in the colon, whereby JMT enriched for jejunal signatures (NES = 1.52, padj = 8.49e−5) and FMT enhanced colonic signatures (NES = 2.48, padj = 3.35e−16) (Figure 5G). JMT had a greater effect in driving jejunal signatures in the jejunum and the FMT better drove colonic signatures in the colon (padj = e−22 and e−16, respectively). Visualization of these genes confirmed enhancement of jejunal and colonic programs after JMT and FMT, respectively.

Given the role of GATA4 in regulating small intestinal identity[31,32] and SATB2[29] in regulating colonic identity, we explored whether protein levels of these transcriptional regulators were also increased upon JMT or FMT via western blot (WB) and immunohistochemistry (IHC) at 1 month post transplant (Figure S6). Based on WB, we observed that JMT enhanced GATA4 protein levels compared with PBS controls ($p = 0.01$) in the jejunum, and FMT enhanced SATB2 levels compared with PBS controls ($p = 0.01$) in the colon (Figure S6). Interestingly, subsets of jejunal crypt cells revealed expression of SATB2, whereas colonic crypts exhibited increased GATA4 levels by IHC, respectively, suggesting progression toward an altered regional identity that may allow for enhanced colonization in non-native environments. These data demonstrate that microbiota enhance regional ecosystems of their native environments (JMT in the jejunum, FMT in the colon) and suppress non-native regional ecosystems to better align with their indigenous environments.

Human FMTs also lead to persistent colonic anaerobes in upper small intestine and reprogramming of regional ecosystems conducive to their engraftment

Mouse models serve as valuable research tools but, of course, do not recapitulate all aspects of human biology. As such, we examined whether findings from the murine studies could be similarly observed in human tissues. To this end, we undertook two approaches to examine the impact of SB vs. LB microbes on human tissues: (1) primary human jejunal organoids (enteroids) cultured from jejunal biopsies treated with JMT and FMT acellular material and (2) duodenal biopsies from patients before and 1 month after FMT.

Primary human jejunal biopsies ($n = 8$ subjects) cultured *in vitro* were treated with a 10% acellular preparation of human jejunal contents derived from a single jejunostomy donor or fecal slurry as an analog for the JMT and FMT, respectively (Figure 6A). Purified RNA was subjected to RNA-seq and each treatment was compared with its own vehicle control (VEH). Although we did not observe all of the gene signatures marking identity conversion observed in the *in vivo* model—and in humans these genes are not strictly jejunal (olfactomedin [*OLFM4*]; fatty acid binding protein 6 [*FABP6*]; *APOA4*; and alkaline phosphatase intestine [*APLI*]) or colonic (*SATB2*; caudal-type homeobox 2 [*CDX2*]; carbonic anhydrase 1 [*CA1*]; and lactoperoxidase [*LPO*])—identity

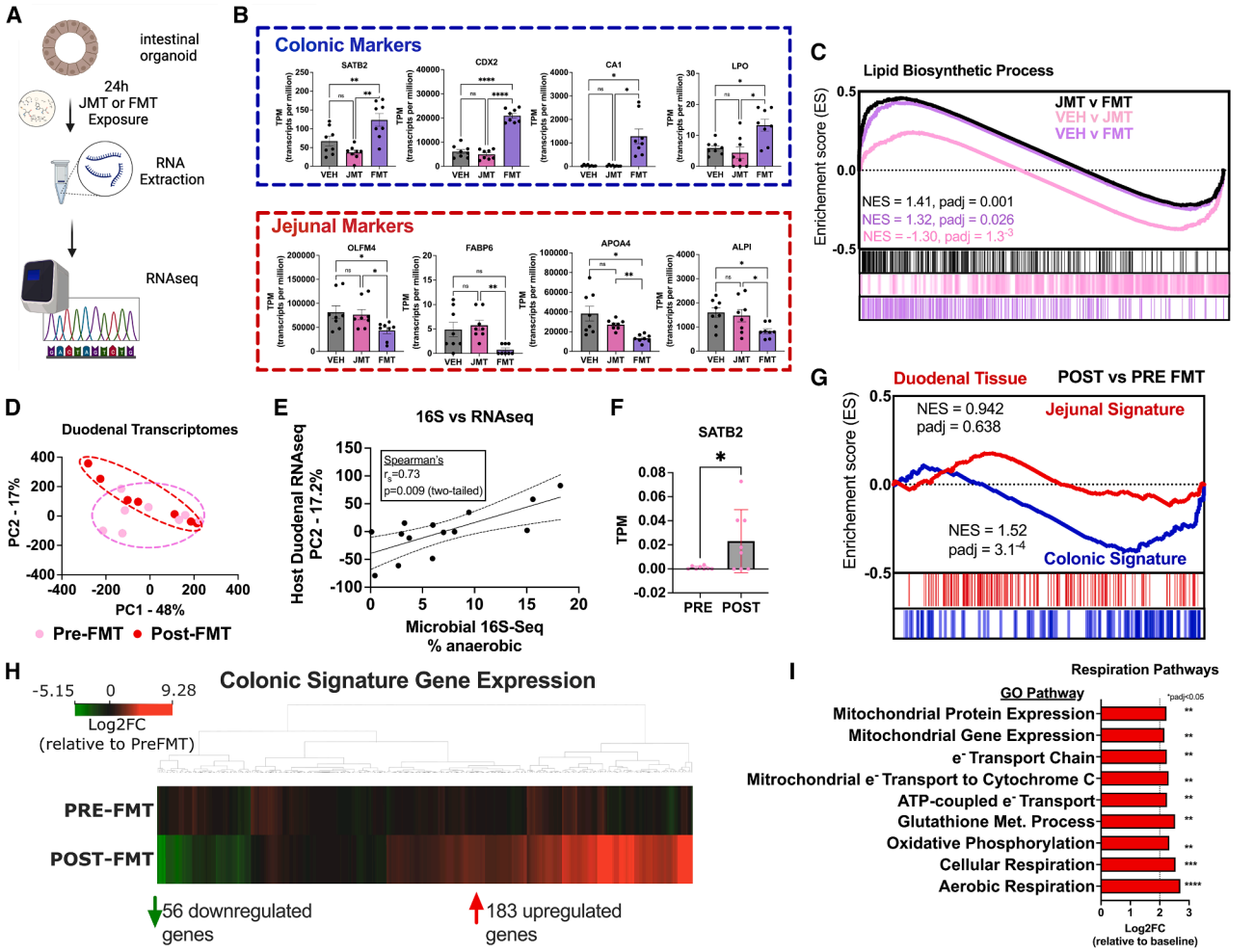

Figure 6. Human tissues reflect metabolic and regional ecosystem shifts

(A) Primary human jejunal biopsies were cultured *in vitro* to generate jejunal enteroids, treated for 24 h with an acellular preparation of human JMT (collected from a jejunostomy bag) or FMT (aspirate from ascending colon), extracted for RNA, and sequenced.

(B) FMT enriched colonic marker genes *SATB2*, *CDX2*, *CA1*, and *LPO*. JMT enriched jejunal marker genes *OLFM4*, *FABP4*, *APOA4*, and *ALPI*, displayed as transcripts per million (TPM, ANOVA, post hoc Tukey's, $*p < 0.05$).

(C) Ranked gene enrichment list for GO pathway "lipid biosynthetic process."

(D) Human FMTs were performed by upper endoscopy and delivered to the terminal duodenum ($n = 7$ subjects). RNA-seq and 16S rRNA sequencing was performed on human duodenal biopsies taken before delivery of the FMT and 4 weeks post FMT during a follow-up endoscopy. PCA of the duodenal transcriptome revealed no significant changes between pre- and post-FMT (PERMANOVA, Mann-Whitney, $p > 0.05$).

(E) Relative abundance of anaerobes colonizing the duodenal mucosa increased post FMT and correlated to the changes in the duodenal transcriptome (Spearman's r, −0.73; $*p = 0.009$).

(F) *Satb2* expression in pre- and post-FMT duodenal biopsies shown as transcripts per million (TPM) (two-tailed t test, $*p < 0.05$).

(G and H) Gene set enrichment analysis for colonic signature gene samples shows an enrichment post FMT (NES = 1.52, padj = 3.1^{-4}), with an enrichment of 183 colonic genes.

(I) Gene ontology pathway analysis demonstrated that mitochondrial, oxidative phosphorylation, and aerobic respiration pathways were enriched post FMT (fGSEA, GO pathways, $*$padj < 0.05, NES > 2). All error bars indicate ± SD.

signals comparable to the murine model were enhanced within 24 h of JMT and FMT treatment, respectively, suggesting the microbe-mediated shifts between jejunum to colon are not immediate. (Figure 6B; ANOVA, $*p < 0.05$.) Pathway analysis revealed lipid absorption, transport, biosynthesis, and storage pathways, and carbohydrate biosynthesis and usage pathways were enriched in the JMT-treated enteroids (Figure 6C; Data S1). However, pathways related to lipid and carbohydrate metabolism were downregulated in FMT-treated enteroids. Importantly, the "lipid biosynthesis pathway" was enriched in JMT-treated and downregulated in FMT-treated enteroids (Figure 6C), reflecting the ability of SB microbiota to enhance lipid, carbohydrate, and other metabolic processes. Although further work is needed to assess the impact on specific human identity markers, these data corroborate our findings from the *in vivo* mouse models.

To gain further support for the translatability of these findings, we revisited the cohort of FMT subjects in Figure 1 and performed RNA-seq on the tissues ($n = 7$ pre-FMT and $n = 7$ post-FMT).[33,49] Analysis of the duodenal transcriptome revealed no statistical difference between pre- and post-FMT samples (Figure 6D; PERMANOVA, $p > 0.05$). However, we found that changes to the duodenal transcriptome correlated to the increased levels of anaerobic colonization, suggesting interindividual responses depended on FMT engraftment (Spearman's R = 0.73, two-tailed $p = 0.009$) (Figure 6E). We observed increased *SATB2* expression (Student's t test, $^{*}p = 0.39$) and an enriched colonic signature (NES = 1.52, $p$adj = 3.1^{-4}) of 183 upregulated colonic genes (Figures 6F–6H). Pathway analysis revealed increased oxygen consumptive processes within the duodenum, including mitochondrial expression, oxidative phosphorylation, and aerobic respiration (Figure 6I; NES $\geq$ 2, $p$adj < 0.05). Increases in oxygen consumption within the small intestine could reduce luminal oxygen levels and support a more anaerobic environment, permitting anaerobic colonization.[45] Together, these data corroborate our murine studies, supporting the finding that microbes are able to shift mucosal ecosystems to fit their native environment's signature and that these processes can occur in humans.

DISCUSSION

FMTs are performed in clinic with little consideration for reconstitution of regional microbiomes outside of the colon that are unique and distinct.[15,16] Mismatches between post-FMT microbiota and host-gut regional ecosystems have consequences that can be observed clinically and experimentally. The increased engraftment by colonic anaerobes in the duodenum of post-FMT patients provided support that mismatches of gut microbiota in non-indigenous regional gut ecosystems do take place. When investigated further, our post-antibiotic microbial transplant mouse model allowed us to define the consequences of different types of MTs. We now show that FMTs can cause sustained regional microbe-to-host mismatches. Microbes from FMTs successfully engrafted all regions of the gut, despite showing preference for their indigenous microbial habitat and caused restructuring of the local microbiome community membership through engraftment in the SB (Mann-Whitney, $p < 0.05$ all pairwise comparisons). Importantly, functional output of the microbiota is altered after MT, shifting BA species, carbohydrate, and amino acid levels in both regional gut and systemic metabolite pools. Changes that arise from microbial mismatches affected energy balance and hepatic transcription, which persisted up to 3 months after only one MT treatment. JMT primarily impacted host metabolic pathways and FMT largely affected immune pathways—highlighting the dichotomous impact of these two donor populations. JMT enrichment of total levels of BAs within the gut corresponds to the increased expression of fatty acid transporters in the intestine and fat absorption pathways, lowered energy expenditure, and increased weight gain (Figures 2F, 4E, 4G, and 4K).

Effects on the host may be tied to the ability of microbes to alter their regional gut ecosystems. Host control of microbial colonization is well appreciated from human studies,[50–52] QTL mapping of variants that restrict bacterial strains,[53,54] and the ability of a GF mouse to affect an anaerobic colon.[45] However, these data argue that the final gut ecosystem is a product of crosstalk between the host and the microbes present. JMT enriched for known regulators of jejunal identity, *Gata4* and *Gata6*, and FMT enhanced the expression of *Satb2*, a known master regulator of colonic identity (Figure 5). These affected a large transcriptional skew toward jejunal or colonic programs, respectively, suggesting that microbes condition their regional ecosystems to create a more hospitable environment. Particularly for strict anaerobes, actively enhancing host oxygen consumption through lipid oxidation or raising total respiration would be an attractive mechanism to reduce luminal oxygen and increase colonization. It is interesting to note that although JMTs and FMTs affected transcription in both the jejunum and colon, enrichment effect sizes were higher during cases of microbe-to-region match, likely due to the levels of microbial colonization. Whether raising the level of engraftment enhances these effects through repeat administration of MT, whether these changes are reversible, and identification of specific microbes and effector molecules are all important questions to inform future therapies.

Importantly, we see similar changes in our human tissue models, including signatures of shifted identity corresponding to increased anaerobic colonization and changes to oxygen utilization pathways. Human FMT specifically recapitulated the increased levels of anaerobic microbe colonization, expression of *SATB2* and colonic identity, and the enrichment of oxygen consumptive processes but not the major metabolic pathway shifts. This may be due to the nature of the duodenum being less important for nutrient absorption. Institutional Review Board (IRB) approval to perform an elective FMT, with no indication to perform a double balloon to access the jejunum, and to do so twice, would not be justified. From the organoid model, we can conclude that human jejunal tissues replicate many of these metabolic shifts, which can occur quickly (within 24 h) and in the absence of actual microbes. Shifts in the identity of the tissues, as seen in the *in vivo* mouse model, and in human FMTs may suggest that persistent colonization of microbes is required, perhaps through the continuous exposure to altered metabolites.

Lineage enhancement with matched microbiota demonstrates the ability of microbes to drive the regional intestinal identity. These data suggest that lineage switching during cases of mismatch is partial at 1 month after transplant. Changes in regional identity are coordinated across multiple tissue systems, including epithelium and stroma,[55] and could also be influenced by the nature of the luminal flow and tissue biomechanics.[56,57] To this list of lineage determinants, our study shows that the microbiome is a contributory, but also therapeutically accessible, factor. Transdifferentiation phenomena in the clinic[58] and in murine models[59,60] show that intestinalization is usually not complete and may exhibit variegated phenotypes. Nonetheless, the metaplastic-like tissue can still have profound physiological and pathophysiological effects. Further work will need to evaluate whether a JMT-treated colon has true functional hallmarks of SB and the FMT-treated jejunum has verified colonic conversion, which can be supported by the use and characterization of genetic models (e.g., SATB2 and GATA4 intestinal knockouts). Furthermore,

identification of the specific microbiota able to drive these changes and their mediators through culture'omics is required.

These data raise a cautionary note, that unrecognized short- and long-term consequences of the FMT may emerge in clinical practice, in particular for off-label use where mechanism and efficacy remain unknown. Currently, safety and efficacy are mostly gauged by clinical symptoms and desired outcomes. Few studies employ more objective measures that include multi'omic assessments of both host and gut microbiota that could reveal changes that may not yet be clinically manifested. Lack of specific SBM may be a cause of outcome failures and promote non-physiological shifts in intestinal regional ecosystems and systemic metabolism and immunity. At the very least, these data demonstrate that fecal microbiota that normally comprise FMTs are not sufficient to reconstitute the entire gut and can cause undesired, off-target effects. Although this study focused on the consequences of SBM and LBM mismatches, CMT that are admixtures of SBM and LBM best approximated the liver transcriptome of healthy, SPF mice (see Data S1). SB metabolomic profiles mirrored JMT and colonic metabolomic profiles mirrored FMT (Figure 2C). Metabolically, CMT recipients displayed the highest levels of energy expenditure and activity, expressed robust lipid oxidation, and gained the least weight (Figure 4). Rather than FMTs, this advocates the need to incorporate therapies encompassing SBM and LBM or an omni-microbial transplant (OMT).

In conclusion, our results show that regional microbial engraftment mismatches can arise during FMT and have negative consequences for host health and metabolism, altering the fundamental nature and identity of regional gut ecosystems. These data strongly support the need for more objective measures to assess short- and long-term consequences of FMTs and will likely inform future microbiome-based interventions (MBIs) to consider both the SB and LB environments and the microbes within each. In addition, further scrutiny should be placed on the optimal route of FMT delivery, whether via the oral route or upper endoscopy as compared with colonoscopy. The latter may help prevent potential off-target consequences described herein.

Limitations of the study

Although this study demonstrates the important and distinct impacts of SBM vs. LBM on host physiology, study limitations leave certain questions unanswered for future studies. First, the number of human samples obtained was limited, examined for a time period of 1 month after transplantation, and taken during upper endoscopy, namely duodenal tissues. A prospective study examining whether changes to the intestinal mucosa persist beyond 1 month in humans, and patient-matched biopsies from the colon and deeper into the SB, would provide a direct comparison with the changes observed in our murine models—as would collection from healthy individuals, despite the challenges of undergoing these procedures without the medical indication. Second, the techniques employed to examine changes to the microbiome and host tissues are predominated by bulk-omics methodologies, despite our understanding that there is biologically relevant architecture of the microbiota and intestinal mucosa. Therefore, resolving the spatial distribution of specific bacteria, their metabolite distributions, and the responses of specific cell types is important in identifying the major microbial components responsible for the changes in cell lineage observed in this study and the underlying mechanisms. Future studies will also focus on determining the long-term implications of FMT on host metabolism and immune function, such as after 6 months to 1 year post transplant, and the effects on other organ systems, including the brain.

RESOURCE AVAILABILITY

Lead contact

Further information and requests for resources and reagents should be directed to, and will be fulfilled by, the lead contact, Eugene B. Chang (echang@bsd.uchicago.edu).

Materials availability

This study did not generate new unique reagents.

Data and code availability

The data will be shared by the lead contact upon request.

- All metabolomics data were submitted to MassIVE and are publicly available under accession number MassIVE: MSV000097448.
- All 16S rRNA sequencing data, shotgun metagenomic data, and RNA-seq data were submitted to the Sequence Read Archive (SRA) under project accession number SRA: PRJNA1223841, with all relevant and de-identified metadata included with each submission.

ACKNOWLEDGMENTS

This work was supported by NIH-NIDDK-1R01DK138072, the University of Chicago Center for Interdisciplinary Study of Intestinal Inflammatory Disorders (C-IID, NIDDK P30 DK042086), and the University of Chicago GI Research Foundation (GIRF, IC20240001). O.D., J.L., and J.C. were supported by 2T32DK007074-47.

AUTHOR CONTRIBUTIONS

E.C., K.M., D.R., O.D., and M.M. conceptualized and designed this study. O.D. and M.M. performed the mouse experiments, with assistance from C.C., A.T., H.C., J.C., M.S., J.K., J.L., M.C., and J.M. O.D. and J.K. performed the human organoid experiments, with assistance from M.S. and C.C. J.X., M.C., C.L., and O.D. performed the immunohistochemistry. A.S.M. provided interpretation and analysis of the metabolomics data. S.K. performed the western blotting. O.D. and M.M. analyzed the data. Z.X., S.N., F.C., and H.T. performed the human FMT and collected, processed, and sequenced the samples. O.D. analyzed the data. K.M. and E.C. supervised the project. E.C., O.D., M.M., and K.M. wrote the manuscript. All authors contributed to the editing of the manuscript.

DECLARATION OF INTERESTS

The authors declare no competing interests.

STAR★METHODS

Detailed methods are provided in the online version of this paper and include the following:

- KEY RESOURCES TABLE
- EXPERIMENTAL MODEL AND STUDY PARTICIPANT DETAILS
  - Animal Models
  - Human Subjects
- METHOD DETAILS
  - 16S rRNA sequencing
  - Shotgun sequencing and cross'omics with host transcriptional data
  - Metabolomics

SUPPLEMENTAL INFORMATION

Supplemental information can be found online at https://doi.org/10.1016/j.cell.2025.05.014.

Received: May 10, 2024
Revised: November 12, 2024
Accepted: May 15, 2025
Published: June 6, 2025

REFERENCES

1. Bartlett, J.G. (2002). Clinical practice. Antibiotic-Associated Diarrhea. N. Engl. J. Med. *346*, 334–339. https://doi.org/10.1056/NEJMcp011603.
2. Baunwall, S.M.D., Lee, M.M., Eriksen, M.K., Mullish, B.H., Marchesi, J.R., Dahlerup, J.F., and Hvas, C.L. (2020). Faecal microbiota transplantation for recurrent Clostridioides difficile infection: An updated systematic review and meta-analysis. EClinicalmedicine *29–30*, 100642. https://doi.org/10.1016/j.eclinm.2020.100642.
3. Ianiro, G., Bibbò, S., Porcari, S., Settanni, C.R., Giambò, F., Curta, A.R., Quaranta, G., Scaldaferri, F., Masucci, L., Sanguinetti, M., et al. (2021). Fecal microbiota transplantation for recurrent C. difficile infection in patients with inflammatory bowel disease: experience of a large-volume European FMT center. Gut Microbes *13*, 1994834. https://doi.org/10.1080/19490976.2021.1994834.
4. Yadegar, A., Pakpoor, S., Ibrahim, F.F., Nabavi-Rad, A., Cook, L., Walter, J., Seekatz, A.M., Wong, K., Monaghan, T.M., and Kao, D. (2023). Beneficial effects of fecal microbiota transplantation in recurrent Clostridioides difficile infection. Cell Host Microbe *31*, 695–711. https://doi.org/10.1016/j.chom.2023.03.019.
5. Zhang, J., Zhu, G., Wan, L., Liang, Y., Liu, X., Yan, H., Zhang, B., and Yang, G. (2023). Effect of fecal microbiota transplantation in children with autism spectrum disorder: A systematic review. Front. Psychiatry *14*, 1123658. https://doi.org/10.3389/fpsyt.2023.1123658.
6. Feng, J., Chen, Y., Liu, Y., Lin, L., Lin, X., Gong, W., Xia, R., He, J., Sheng, J., Cai, H., et al. (2023). Efficacy and safety of fecal microbiota transplantation in the treatment of ulcerative colitis: a systematic review and meta-analysis. Sci. Rep. *13*, 14494. https://doi.org/10.1038/s41598-023-41182-6.
7. Kootte, R.S., Levin, E., Salojärvi, J., Smits, L.P., Hartstra, A.V., Udayappan, S.D., Hermes, G., Bouter, K.E., Koopen, A.M., Holst, J.J., et al. (2017). Improvement of Insulin Sensitivity after Lean Donor Feces in Metabolic Syndrome Is Driven by Baseline Intestinal Microbiota Composition. Cell Metab. *26*, 611–619.e6. https://doi.org/10.1016/j.cmet.2017.09.008.
8. Davar, D., Dzutsev, A.K., McCulloch, J.A., Rodrigues, R.R., Chauvin, J.-M., Morrison, R.M., Deblasio, R.N., Menna, C., Ding, Q., Pagliano, O., et al. (2021). Fecal microbiota transplant overcomes resistance to anti–PD-1 therapy in melanoma patients. Science *371*, 595–602. https://doi.org/10.1126/science.abf3363.
9. Routy, B., Lenehan, J.G., Miller, W.H., Jamal, R., Messaoudene, M., Daisley, B.A., Hes, C., Al, K.F., Martinez-Gili, L., Punčochář, M., et al. (2023). Fecal microbiota transplantation plus anti-PD-1 immunotherapy in advanced melanoma: a phase I trial. Nat. Med. *29*, 2121–2132. https://doi.org/10.1038/s41591-023-02453-x.
10. Baruch, E.N., Youngster, I., Ben-Betzalel, G., Ortenberg, R., Lahat, A., Katz, L., Adler, K., Dick-Necula, D., Raskin, S., Bloch, N., et al. (2021). Fecal microbiota transplant promotes response in immunotherapy-refractory melanoma patients. Science *371*, 602–609. https://doi.org/10.1126/science.abb5920.
11. Alang, N., and Kelly, C.R. (2015). Weight Gain After Fecal Microbiota Transplantation. Open Forum Infect. Dis. *2*, ofv004. https://doi.org/10.1093/ofid/ofv004.
12. Baxter, M., Ahmad, T., Colville, A., and Sheridan, R. (2015). Fatal Aspiration Pneumonia as a Complication of Fecal Microbiota Transplant. Clin. Infect. Dis. *61*, 136–137. https://doi.org/10.1093/cid/civ247.
13. DeFilipp, Z., Bloom, P.P., Torres Soto, M., Mansour, M.K., Sater, M.R.A., Huntley, M.H., Turbett, S., Chung, R.T., Chen, Y.-B., and Hohmann, E.L. (2019). Drug-Resistant *E. coli* Bacteremia Transmitted by Fecal Microbiota Transplant. N. Engl. J. Med. *381*, 2043–2050. https://doi.org/10.1056/NEJMoa1910437.
14. Alhmoud, T., and Gavin, M. (2014). An Unusual Complication After a Fecal Microbiota Transplant via Colonoscopy: 1431. Off. J. Am. Coll. Gastroenterol. ACG *109*, S424.
15. Shalon, D., Culver, R.N., Grembi, J.A., Folz, J., Treit, P.V., Shi, H., Rosenberger, F.A., Dethlefsen, L., Meng, X., Yaffe, E., et al. (2023). Profiling the human intestinal environment under physiological conditions. Nature *617*, 581–591. https://doi.org/10.1038/s41586-023-05989-7.
16. She, J.-J., Liu, W.-X., Ding, X.-M., Guo, G., Han, J., Shi, F.-Y., Lau, H.C.-H., Ding, C.-G., Xue, W.-J., Shi, W., et al. (2024). Defining the biogeographical map and potential bacterial translocation of microbiome in human 'surface organs.'. Nat. Commun. *15*, 427. https://doi.org/10.1038/s41467-024-44720-6.
17. Chang, E.B., and Martinez-Guryn, K. (2019). Small intestinal microbiota: the neglected stepchild needed for fat digestion and absorption. Gut Microbes *10*, 235–240. https://doi.org/10.1080/19490976.2018.1502539.
18. Martinez-Guryn, K., Hubert, N., Frazier, K., Urlass, S., Musch, M.W., Ojeda, P., Pierre, J.F., Miyoshi, J., Sontag, T.J., Cham, C.M., et al. (2018). Small Intestine Microbiota Regulate Host Digestive and Absorptive Adaptive Responses to Dietary Lipids. Cell Host Microbe *23*, 458–469.e5.. https://doi.org/10.1016/j.chom.2018.03.011.
19. Zoetendal, E.G., Raes, J., Van Den Bogert, B., Arumugam, M., Booijink, C.C.G.M., Troost, F.J., Bork, P., Wels, M., De Vos, W.M., and Kleerebezem, M. (2012). The human small intestinal microbiota is driven by rapid uptake and conversion of simple carbohydrates. ISME J. *6*, 1415–1426. https://doi.org/10.1038/ismej.2011.212.
20. Poteres, E., Hubert, N., Poludasu, S., Brigando, G., Moore, J., Keeler, K., Isabelli, A., Ibay, I.C.V., Alt, L., Pytynia, M., et al. (2020). Selective Regional Alteration of the Gut Microbiota by Diet and Antibiotics. Front. Physiol. *11*, 797. https://doi.org/10.3389/fphys.2020.00797.
21. Leone, V., Gibbons, S.M., Martinez, K., Hutchison, A.L., Huang, E.Y., Cham, C.M., Pierre, J.F., Heneghan, A.F., Nadimpalli, A., Hubert, N., et al. (2015). Effects of Diurnal Variation of Gut Microbes and High-Fat Feeding on Host Circadian Clock Function and Metabolism. Cell Host Microbe *17*, 681–689. https://doi.org/10.1016/j.chom.2015.03.006.
22. Mukherji, A., Kobiita, A., Ye, T., and Chambon, P. (2013). Homeostasis in Intestinal Epithelium Is Orchestrated by the Circadian Clock and Microbiota Cues Transduced by TLRs. Cell *153*, 812–827. https://doi.org/10.1016/j.cell.2013.04.020.
23. Frazier, K., Kambal, A., Zale, E.A., Pierre, J.F., Hubert, N., Miyoshi, S., Miyoshi, J., Ringus, D.L., Harris, D., Yang, K., et al. (2022). High-fat diet disrupts REG3γ and gut microbial rhythms promoting metabolic dysfunction. Cell Host Microbe *30*, 809–823.e6. https://doi.org/10.1016/j.chom.2022.03.030.
24. Martinez-Guryn, K., Leone, V., and Chang, E.B. (2019). Regional Diversity of the Gastrointestinal Microbiome. Cell Host Microbe *26*, 314–324. https://doi.org/10.1016/j.chom.2019.08.011.
25. Donaldson, G.P., Lee, S.M., and Mazmanian, S.K. (2016). Gut biogeography of the bacterial microbiota. Nat. Rev. Microbiol. *14*, 20–32. https://doi.org/10.1038/nrmicro3552.

26. Hickey, J.W., Becker, W.R., Nevins, S.A., Horning, A., Perez, A.E., Zhu, C., Zhu, B., Wei, B., Chiu, R., Chen, D.C., et al. (2023). Organization of the human intestine at single-cell resolution. Nature *619*, 572–584. https://doi.org/10.1038/s41586-023-05915-x.

27. Boland, M. (2016). Human digestion – a processing perspective. J. Sci. Food Agric. *96*, 2275–2283. https://doi.org/10.1002/jsfa.7601.

28. Kahai, P., Mandiga, P., Wehrle, C.J., and Lobo, S. (2024). Anatomy, Abdomen and Pelvis: Large Intestine. StatPearls (StatPearls Publishing).

29. Gu, W., Wang, H., Huang, X., Kraiczy, J., Singh, P.N.P., Ng, C., Dagdeviren, S., Houghton, S., Pellon-Cardenas, O., Lan, Y., et al. (2022). SATB2 preserves colon stem cell identity and mediates ileum-colon conversion via enhancer remodeling. Cell Stem Cell *29*, 101–115.e10. https://doi.org/10.1016/j.stem.2021.09.004.

30. Earley, Z.M., Lisicka, W., Sifakis, J.J., Aguirre-Gamboa, R., Kowalczyk, A., Barlow, J.T., Shaw, D.G., Discepolo, V., Tan, I.L., Gona, S., et al. (2023). GATA4 controls regionalization of tissue immunity and commensal-driven immunopathology. Immunity *56*, 43–57.e10.. https://doi.org/10.1016/j.immuni.2022.12.009.

31. Walker, E.M., Thompson, C.A., Kohlnhofer, B.M., Faber, M.L., and Battle, M.A. (2014). Characterization of the developing small intestine in the absence of either GATA4 or GATA6. BMC Res. Notes *7*, 902. https://doi.org/10.1186/1756-0500-7-902.

32. Thompson, C.A., Wojta, K., Pulakanti, K., Rao, S., Dawson, P., and Battle, M.A. (2017). GATA4 Is Sufficient to Establish Jejunal Versus Ileal Identity in the Small Intestine. Cell. Mol. Gastroenterol. Hepatol. *3*, 422–446. https://doi.org/10.1016/j.jcmgh.2016.12.009.

33. Zhang, F., Zuo, T., Wan, Y., Xu, Z., Cheung, C., Li, A.Y., Zhu, W., Tang, W., Chan, P.K.S., Chan, F.K.L., et al. (2022). Multi-omic analyses identify mucosa bacteria and fecal metabolites associated with weight loss after fecal microbiota transplantation. Innovation (Camb) *3*, 100304. https://doi.org/10.1016/j.xinn.2022.100304.

34. Mocanu, V., Rajaruban, S., Dang, J., Kung, J.Y., Deehan, E.C., and Madsen, K.L. (2021). Repeated Fecal Microbial Transplantations and Antibiotic Pre-Treatment Are Linked to Improved Clinical Response and Remission in Inflammatory Bowel Disease: A Systematic Review and Pooled Proportion Meta-Analysis. J. Clin. Med. *10*, 959. https://doi.org/10.3390/jcm10050959.

35. Borody, T.J., Warren, E.F., Leis, S., Surace, R., and Ashman, O. (2003). Treatment of Ulcerative Colitis Using Fecal Bacteriotherapy. J. Clin. Gastroenterol. *37*, 42–47. https://doi.org/10.1097/00004836-200307000-00012.

36. Chen, H.T., Huang, H.L., Xu, H.M., Luo, Q.L., He, J., Li, Y.Q., Zhou, Y.L., Nie, Y.Q., and Zhou, Y.J. (2020). Fecal microbiota transplantation ameliorates active ulcerative colitis. Exp. Ther. Med. *19*, 2650–2660. https://doi.org/10.3892/etm.2020.8512.

37. Costello, S.P., Hughes, P.A., Waters, O., Bryant, R.V., Vincent, A.D., Blatchford, P., Katsikeros, R., Makanyanga, J., Campaniello, M.A., Mavrangelos, C., et al. (2019). Effect of Fecal Microbiota Transplantation on 8-Week Remission in Patients With Ulcerative Colitis: A Randomized Clinical Trial. JAMA *321*, 156–164. https://doi.org/10.1001/jama.2018.20046.

38. Chen, M., Liu, X.L., Zhang, Y.J., Nie, Y.Z., Wu, K.C., and Shi, Y.Q. (2020). Efficacy and safety of fecal microbiota transplantation by washed preparation in patients with moderate to severely active ulcerative colitis. J. Dig. Dis. *21*, 621–628. https://doi.org/10.1111/1751-2980.12938.

39. Parker, K.D., Albeke, S.E., Gigley, J.P., Goldstein, A.M., and Ward, N.L. (2018). Microbiome Composition in Both Wild-Type and Disease Model Mice Is Heavily Influenced by Mouse Facility. Front. Microbiol. *9*, 1598. https://doi.org/10.3389/fmicb.2018.01598.

40. Folz, J., Culver, R.N., Morales, J.M., Grembi, J., Triadafilopoulos, G., Relman, D.A., Huang, K.C., Shalon, D., and Fiehn, O. (2023). Human metabolome variation along the upper intestinal tract. Nat. Metab. *5*, 777–788. https://doi.org/10.1038/s42255-023-00777-z.

41. Liu, C., Du, M.-X., Xie, L.-S., Wang, W.-Z., Chen, B.-S., Yun, C.-Y., Sun, X.-W., Luo, X., Jiang, Y., Wang, K., et al. (2024). Gut commensal Christensenella minuta modulates host metabolism via acylated secondary bile acids. Nat. Microbiol. *9*, 434–450. https://doi.org/10.1038/s41564-023-01570-0.

42. Collins, S.L., Stine, J.G., Bisanz, J.E., Okafor, C.D., and Patterson, A.D. (2023). Bile acids and the gut microbiota: metabolic interactions and impacts on disease. Nat. Rev. Microbiol. *21*, 236–247. https://doi.org/10.1038/s41579-022-00805-x.

43. Li, M., Van Esch, B.C.A.M., Henricks, P.A.J., Folkerts, G., and Garssen, J. (2018). The Anti-inflammatory Effects of Short Chain Fatty Acids on Lipopolysaccharide- or Tumor Necrosis Factor α-Stimulated Endothelial Cells via Activation of GPR41/43 and Inhibition of HDACs. Front. Pharmacol. *9*, 533. https://doi.org/10.3389/fphar.2018.00533.

44. Bogatyrev, S.R., Rolando, J.C., and Ismagilov, R.F. (2020). Self-reinoculation with fecal flora changes microbiota density and composition leading to an altered bile-acid profile in the mouse small intestine. Microbiome *8*, 19. https://doi.org/10.1186/s40168-020-0785-4.

45. Friedman, E.S., Bittinger, K., Esipova, T.V., Hou, L., Chau, L., Jiang, J., Mesaros, C., Lund, P.J., Liang, X., FitzGerald, G.A., et al. (2018). Microbes vs. chemistry in the origin of the anaerobic gut lumen. Proc. Natl. Acad. Sci. USA *115*, 4170–4175. https://doi.org/10.1073/pnas.1718635115.

46. Fitzgerald, R.J., Gustafsson, B.E., and McDaniel, E.G. (1964). Effects of Coprophagy Prevention on Intestinal Microflora in Rats. J. Nutr. *84*, 155–160. https://doi.org/10.1093/jn/84.2.155.

47. Gustafsson, B.E., and Fitzgerald, R.J. (1960). Alteration in Intestinal Microbial Flora of Rats with Tail Cups to Prevent Coprophagy. Proc. Soc. Exp. Biol. Med. *104*, 319–322. https://doi.org/10.3181/00379727-104-25821.

48. Ebino, K.Y., Yoshinaga, K., Saito, T.R., and Takahashi, K.W. (1988). A simple method for prevention of coprophagy in the mouse. Lab. Anim. *22*, 1–4. https://doi.org/10.1258/002367788780746548.

49. Yau, Y.K., Su, Q., Xu, Z., Tang, W., Ching, J.Y.L., Mak, J.W.Y., Cheung, C. P., Fung, M., Ip, M., Chan, P.K.S., et al. (2023). Randomised clinical trial: Faecal microbiota transplantation for irritable bowel syndrome with diarrhoea. Aliment. Pharmacol. Ther. *58*, 795–804. https://doi.org/10.1111/apt.17703.

50. Goodrich, J.K., Davenport, E.R., Beaumont, M., Jackson, M.A., Knight, R., Ober, C., Spector, T.D., Bell, J.T., Clark, A.G., and Ley, R.E. (2016). Genetic Determinants of the Gut Microbiome in UK Twins. Cell Host Microbe *19*, 731–743. https://doi.org/10.1016/j.chom.2016.04.017.

51. Goodrich, J.K., Waters, J.L., Poole, A.C., Sutter, J.L., Koren, O., Blekhman, R., Beaumont, M., Van Treuren, W., Knight, R., Bell, J.T., et al. (2014). Human Genetics Shape the Gut Microbiome. Cell *159*, 789–799. https://doi.org/10.1016/j.cell.2014.09.053.

52. Benson, A.K., Kelly, S.A., Legge, R., Ma, F., Low, S.J., Kim, J., Zhang, M., Oh, P.L., Nehrenberg, D., Hua, K., et al. (2010). Individuality in gut microbiota composition is a complex polygenic trait shaped by multiple environmental and host genetic factors. Proc. Natl. Acad. Sci. USA *107*, 18933–18938. https://doi.org/10.1073/pnas.1007028107.

53. Bubier, J.A., Chesler, E.J., and Weinstock, G.M. (2021). Host genetic control of gut microbiome composition. Mamm. Genome *32*, 263–281. https://doi.org/10.1007/s00335-021-09884-2.

54. Zhang, Q., Linke, V., Overmyer, K.A., Traeger, L.L., Kasahara, K., Miller, I. J., Manson, D.E., Polaske, T.J., Kerby, R.L., Kemis, J.H., et al. (2023). Genetic mapping of microbial and host traits reveals production of immunomodulatory lipids by Akkermansia muciniphila in the murine gut. Nat. Microbiol. *8*, 424–440. https://doi.org/10.1038/s41564-023-01326-w.

55. Elmentaite, R., Kumasaka, N., Roberts, K., Fleming, A., Dann, E., King, H. W., Kleshchevnikov, V., Dabrowska, M., Pritchard, S., Bolt, L., et al. (2021). Cells of the human intestinal tract mapped across space and time. Nature *597*, 250–255. https://doi.org/10.1038/s41586-021-03852-1.

56. Huycke, T.R., Häkkinen, T.J., Miyazaki, H., Srivastava, V., Barruet, E., McGinnis, C.S., Kalantari, A., Cornwall-Scoones, J., Vaka, D., Zhu, Q.,

et al. (2024). Patterning and folding of intestinal villi by active mesenchymal dewetting. Cell *187*, 3072–3089.e20. https://doi.org/10.1016/j.cell.2024.04.039.

57. Houtekamer, R.M., Van Der Net, M.C., Maurice, M.M., and Gloerich, M. (2022). Mechanical forces directing intestinal form and function. Curr. Biol. *32*, R791–R805. https://doi.org/10.1016/j.cub.2022.05.041.
58. Paull, A., Trier, J.S., Dalton, M.D., Camp, R.C., Loeb, P., and Goyal, R.K. (1976). The Histologic Spectrum of Barrett's Esophagus. N. Engl. J. Med. *295*, 476–480. https://doi.org/10.1056/NEJM197608262950904.
59. Liu, C.Y., Girish, N., Gomez, M.L., Dubé, P.E., Washington, M.K., Simons, B.D., and Polk, D.B. (2022). Transitional Anal Cells Mediate Colonic Re-epithelialization in Colitis. Gastroenterology *162*, 1975–1989. https://doi.org/10.1053/j.gastro.2022.02.031.
60. Bockerstett, K.A., Lewis, S.A., Wolf, K.J., Noto, C.N., Jackson, N.M., Ford, E.L., Ahn, T.-H., and DiPaolo, R.J. (2020). Single-cell transcriptional analyses of spasmolytic polypeptide-expressing metaplasia arising from acute drug injury and chronic inflammation in the stomach. Gut *69*, 1027–1038. https://doi.org/10.1136/gutjnl-2019-318930.
61. Bolyen, E., Rideout, J.R., Dillon, M.R., Bokulich, N.A., Abnet, C.C., Al-Ghalith, G.A., Alexander, H., Alm, E.J., Arumugam, M., Asnicar, F., et al. (2019). Reproducible, interactive, scalable and extensible microbiome data science using QIIME 2. Nat. Biotechnol. *37*, 852–857. https://doi.org/10.1038/s41587-019-0209-9.
62. Eren, A.M., Esen, Ö.C., Quince, C., Vineis, J.H., Morrison, H.G., Sogin, M.L., and Delmont, T.O. (2015). Anvi'o: an advanced analysis and visualization platform for 'omics data. PeerJ *3*, e1319. https://doi.org/10.7717/peerj.1319.
63. Mallick, H., Rahnavard, A., McIver, L.J., Ma, S., Zhang, Y., Nguyen, L.H., Tickle, T.L., Weingart, G., Ren, B., Schwager, E.H., et al. (2021). Multivariable association discovery in population-scale meta-omics studies. PLOS Comput. Biol. *17*, e1009442. https://doi.org/10.1371/journal.pcbi.1009442.
64. Love, M.I., Huber, W., and Anders, S. (2014). Moderated estimation of fold change and dispersion for RNA-seq data with DESeq2. Genome Biol. *15*, 550. https://doi.org/10.1186/s13059-014-0550-8.
65. Bolger, A.M., Lohse, M., and Usadel, B. (2014). Trimmomatic: a flexible trimmer for Illumina sequence data. Bioinformatics *30*, 2114–2120. https://doi.org/10.1093/bioinformatics/btu170.
66. Dobin, A., Davis, C.A., Schlesinger, F., Drenkow, J., Zaleski, C., Jha, S., Batut, P., Chaisson, M., and Gingeras, T.R. (2013). STAR: ultrafast universal RNA-seq aligner. Bioinformatics *29*, 15–21. https://doi.org/10.1093/bioinformatics/bts635.
67. Shi, W. (2017). Rsubread: an R/Bioconductor package for alignment and quantification of RNA sequencing reads (Bioconductor) https://doi.org/10.18129/B9.BIOC.RSUBREAD.
68. Leek, J.T. (2017). sva: Surrogate Variable Analysis (Bioconductor) https://doi.org/10.18129/B9.BIOC.SVA.
69. Mootha, V.K., Lindgren, C.M., Eriksson, K.-F., Subramanian, A., Sihag, S., Lehar, J., Puigserver, P., Carlsson, E., Ridderstråle, M., Laurila, E., et al. (2003). PGC-1α-responsive genes involved in oxidative phosphorylation are coordinately downregulated in human diabetes. Nat. Genet. *34*, 267–273. https://doi.org/10.1038/ng1180.
70. Subramanian, A., Tamayo, P., Mootha, V.K., Mukherjee, S., Ebert, B.L., Gillette, M.A., Paulovich, A., Pomeroy, S.L., Golub, T.R., Lander, E.S., et al. (2005). Gene set enrichment analysis: A knowledge-based approach for interpreting genome-wide expression profiles. Proc. Natl. Acad. Sci. USA *102*, 15545–15550. https://doi.org/10.1073/pnas.0506580102.
71. Waskom, M. (2021). seaborn: statistical data visualization. J. Open Source Softw. *6*, 3021. https://doi.org/10.21105/joss.03021.
72. Miyoshi, J., Leone, V., Nobutani, K., Musch, M.W., Martinez-Guryn, K., Wang, Y., Miyoshi, S., Bobe, A.M., Eren, A.M., and Chang, E.B. (2018). Minimizing confounders and increasing data quality in murine models for studies of the gut microbiome. PeerJ *6*, e5166. https://doi.org/10.7717/peerj.5166.
73. Sato, T., Stange, D.E., Ferrante, M., Vries, R.G.J., Van Es, J.H., Van Den Brink, S., Van Houdt, W.J., Pronk, A., Van Gorp, J., Siersema, P.D., et al. (2011). Long-term Expansion of Epithelial Organoids From Human Colon, Adenoma, Adenocarcinoma, and Barrett's Epithelium. Gastroenterology *141*, 1762–1772. https://doi.org/10.1053/j.gastro.2011.07.050.
74. Segata, N., Izard, J., Waldron, L., Gevers, D., Miropolsky, L., Garrett, W.S., and Huttenhower, C. (2011). Metagenomic biomarker discovery and explanation. Genome Biol. *12*, R60. https://doi.org/10.1186/gb-2011-12-6-r60.
75. Priya, S., Burns, M.B., Ward, T., Mars, R.A.T., Adamowicz, B., Lock, E.F., Kashyap, P.C., Knights, D., and Blekhman, R. (2022). Identification of shared and disease-specific host gene–microbiome associations across human diseases using multi-omic integration. Nat. Microbiol. *7*, 780–795. https://doi.org/10.1038/s41564-022-01121-z.
76. Haak, B.W., Littmann, E.R., Chaubard, J.-L., Pickard, A.J., Fontana, E., Adhi, F., Gyaltshen, Y., Ling, L., Morjaria, S.M., Peled, J.U., et al. (2018). Impact of gut colonization with butyrate producing microbiota on respiratory viral infection following allo-HCT. Blood, blood-2018-01-828996. Blood *131*, 2978–2986. https://doi.org/10.1182/blood-2018-01-828996.
77. Shan, J., Peng, L., Qian, W., Xie, T., Kang, A., Gao, B., and Di, L. (2018). Integrated Serum and Fecal Metabolomics Study of Collagen-Induced Arthritis Rats and the Therapeutic Effects of the Zushima Tablet. Front. Pharmacol. *9*, 891. https://doi.org/10.3389/fphar.2018.00891.
78. Fiehn, O. (2016). Metabolomics by Gas Chromatography–Mass Spectrometry: Combined Targeted and Untargeted Profiling. Curr. Protoc. Mol. Biol. *114*, 30.4.1–30.4.32. https://doi.org/10.1002/0471142727.mb3004s114.
79. Gómez, C., Stücheli, S., Kratschmar, D.V., Bouitbir, J., and Odermatt, A. (2020). Development and Validation of a Highly Sensitive LC-MS/MS Method for the Analysis of Bile Acids in Serum, Plasma, and Liver Tissue Samples. Metabolites *10*, 282. https://doi.org/10.3390/metabo10070282.
80. Weir, J.B. (1990). New methods for calculating metabolic rate with special reference to protein metabolism. 1949. Nutrition *6*, 213–221.
81. Riachi, M., Himms-Hagen, J., and Harper, M.-E. (2004). Percent relative cumulative frequency analysis in indirect calorimetry: application to studies of transgenic mice. Can. J. Physiol. Pharmacol. *82*, 1075–1083. https://doi.org/10.1139/y04-117.

STAR★METHODS

KEY RESOURCES TABLE

REAGENT or RESOURCE	SOURCE	IDENTIFIER
Antibodies		
anti-Gata4	Abcam	Cat#ab307823; RRID:AB_3105880
anti-Satb2	Abcam	Cat #ab92446; RRID:AB_10563678
StarBright Blue 700 anti-Rb	Bio-rad	Cat#12004162; RRID:AB_2721073
hFAB Rhodamine anti-actin	Bio-rad	Cat#12004164; RRID:AB_2861334
Biological samples		
Human: Jejunal Contents from a single patient with a jejunostomy bag	UChicago Hospital and UChicago Center for Interdisciplinary Study of Inflammatory Intestinal Disorders (C-IID)	IRB 15573A; RRID:SCR_015601
Human: Colon Contents (ascending colon) from a single patient undergoing colonoscopy	UChicago Hospital and UChicago Center for Interdisciplinary Study of Inflammatory Intestinal Disorders (C-IID)	IRB 15573A; RRID_SCR_015601
Chemicals, peptides, and recombinant proteins		
Trizol Reagent	ThermoFisher	155596018
DNase I	Roche	4716728001
Reduced Growth Factor Matrigel	Corning	CLS356231
Advanced DMEM/F12	Life Technologies	11320033
Neomycin sulfate	Goldbio	N-620-5
Vancomycin hydrochloride	Goldbio	V-200-25
Ampicillin sodium	Goldbio	A-301-25
Metronidazole	Goldbio	M-295-100
EDTA (0.5 M)	ThermoFisher	AM9260G
DPBS, no calcium, no magnesium	ThermoFisher	14190136
HALT protease/phosphatase inhibitor	Thermo Scientific	cat#78441
Midi-Protean TGX gels	Bio-rad	cat#5678043
Immun-Blot LF-PVDF	Bio-rad	cat#1620264
ImmPRESS Polymer Reagents	Vector Laboratories	MP-7452, MP-7402
VOP substrate kit	Vector Laboratories	SK-4605
Critical commercial assays		
QiaAmpPowerFecal Pro DNA	Qiagen	51804
RNA Clean & Concentrator + DNase -5	Zymo Research	R1014
QIASeq 1-step amplicon kit	Qiagen	180419
Deposited data		
Mouse, human organoid and human RNA-seq, 16S rRNA, and shotgun metagenomic data	This paper	SRA: PRJNA1223841
Mouse intestinal contents and plasma metabolomics	This paper	MassIVE: MSV000097448
Experimental models: Cell lines		
Human: Primary Enteroid (Jejunum) Lines	UChicago Hospital and UChicago Center for Interdisciplinary Study of Inflammatory Intestinal Disorders (C-IID), Tissue Engineering and Cell Models Core	IRB 15573A; RRID:SCR_015604

(*Continued on next page*)

Continued

REAGENT or RESOURCE	SOURCE	IDENTIFIER
Experimental models: Organisms/strains		
Mouse: WT C57BL/6J	Jackson Labs	RRID:IMSR_JAX:000664
Mouse: WT C57BL/6J	UChicago Chang Lab Mouse Colony	N/A
Mouse: Germ-free (GF) C57BL/6J	UChicago Gnotobiotic Research Animal Facility (GRAF)	RRID:SCR_015603
Human: Primary Duodenum Biopsies	Chinese University of Hong Kong	Clinical Trial Registry NCT03789461
Oligonucleotides		
16S V4-V5 520-FWD AYTGGGYDTAAAGNG	Integrated DNA Technologies (IDT)	N/A
16S V4-V5 909-REV CCGTCAATTYHTTTRAGT	Integrated DNA Technologies (IDT)	N/A
Software and algorithms		
QIIME2 v2022.11	Bolyen et al.[61]	https://qiime2.org
anvio v7.1	Eren et al.[62]	https://anvio.org
MassHunter vB.10	Agilent Technologies	https://agilent.com
MaAsLin2	Mallick et al.[63]	https://www.bioconductor.org/packages/release/bioc/html/Maaslin2.html
'DESeq2'	Love et al.[64]	https://github.com/thelovelab/DESeq2
Trimmomatic, v0.39	Bolger et al.[65]	https://usadellab.org
STAR v2.7.10	Dobin et al.[66]	https://anaconda.org/bioconda/star
'subread' v.2.0.6	Shi et al.[67]	https://bioconductor.org/packages/release/bioc/html/Rsubread.html
'sva'	Leek et al.[68]	https://bioconductor.org/packages/release/bioc/html/sva.html
fGSEA	Mootha et al.[69] and Subramanian et al.[70]	https://bioconductor.org/packages/release/bioc/html/fgsea.html
IM3 software v.21.0.2	Sable Systems	https://sablesys.com
Prism v10	GraphPad	https://graphpad.com
Orange v3.2	open source	https://orangedatamining.com
'*seaborn*'	Waskom et al.[71]	https://seaborn.pydata.org
Inkscape	open source	https://inkscape.org

EXPERIMENTAL MODEL AND STUDY PARTICIPANT DETAILS

Animal Models

All murine experimental procedures were approved by the University of Chicago Institutional Animal Care and Use Committee (IACUC). C57BL/6 mice were bred and maintained under standard 12:12 h light/dark conditions at the University of Chicago. Age and litter-matched specific pathogen free (SPF) or germ free (GF) male C57Bl/6 mice between 8–12 weeks old were randomized into experimental groups and co-housed in standard cage racks in corn cob bedding. All GF mice were bred in germ-free isolators and housed in IsoP sterile caging during experimentation with pine shavings. Mice were fed a standard chow diet (Envigo 2018S). Gnotobiotic diets were gamma irradiated at a dose of 20–50kGy. and tested for sterility prior to use. Small and large bowel microbiota transplant material was obtained from strain, sex, and age matched mice from our University of Chicago colony. N=10 animals per experiment were used as transplant material for n=7 JMT, FMT, and CMT animals. At time of humane euthanasia, contents from the jejunum, cecum and colon were collected and stored in nitrogen flushed containers and pre-reduced saline with 10% glycerol. Contents were then prepared in anaerobic conditions for cecal and colonic material and aerobic conditions for jejunal material, pooled and flash frozen with N_2(l) and stored at -80°C.

Transplant recipients were ordered from Jackson Labs (JAX) at 6 weeks of age and co-housed (n=3-5 per cage). Upon arrival to the University of Chicago animal facility, bedding was pooled and redistributed 2x/week for two weeks to normalize their microbiota compositions described by Miyoshi et al.[72] 100μL of an antibiotic cocktail (ampicillin 1mg/mL, neomycin 1mg/mL, metronidazole 1mg/mL, and vancomycin 0.5mg/mL) was administered daily for 14 days. Animals were given a 48 h recovery period before administration of 200μL JMT, CMT, FMT, or saline control by oral gavage. At time of transplant, aliquots of frozen preparation were resuspended with 2 equivalents of sterile phosphate buffered saline (*m/v*), centrifuged 2min at 500x*g* to remove debris, and the supernatant collected. FMT and CMT material was diluted 1:10 with sterile saline to approximate the difference in CFUs between the small

and large bowel and used immediately. At time of sacrifice, mice were CO_2(g)-asphyxiated followed by exsanguination and cervical dislocation. Plasma and collected tissues were snap-frozen with N_2(l) and stored at −80°C. Beginning at the base of the stomach, the proximal 4 cm of the small intestine was collected as the duodenum. The next 2 cm were disposed, and the following 6 cm were collected as the jejunum. Ileum was harvested beginning at 8 cm proximal to the cecum where the most distal 2 cm were disposed.

Human Subjects

Intestinal samples used to generate enteroids and the jejunal and colonic contents used as "JMT" and "FMT were obtained at the University of Chicago Hospital. Study subjects at University of Chicago were recruited prior to undergoing double balloon endoscopy or colonoscopy at the University of Chicago Medical Center, collected, and banked at the University of Chicago Center for Interdisciplinary study of Intestinal Inflammatory Disorders (C-IID) Organoid Core. Tissue collection from subjects is approved by the University of Chicago Institutional Review Board under 15573A. Written, informed consent was obtained from all participants. Upon collection, deidentified biopsy tissue was immediately placed in ice-cold transport media, then brought to the Chang lab where it was treated and cultured as detailed per Sato et al.[73] and described below. Luminal aspirates were also collected at the time of endoscopy or colonoscopy (collected from the ascending colon), mixed 1:1 with a 2xPBS, 20% glycerol (*v/v*) (final 1xPBS, 10% glycerol), and stored immediately at -80°C.

Deidentified duodenal biopsies used for 16S analysis and RNAseq were consented and obtained at the Chinese University of Hong Kong and were participants in a previous study studying FMT as a potential obesity therapy.[33] The study was approved by the Joint Chinese University of Hong Kong-New Territories East Cluster Clinical Research Ethics Committee (The Joint CUHK-NTEC CREC, CREC ref. no. 2018.444, Clinical Trial Registry, NCT03789461).

METHOD DETAILS

16S rRNA sequencing

16S rRNA sequencing was performed at the University of Chicago Duchossois Family Institute in the Microbiome Metagenomics Facility (DFI MMF). DNA extraction from intestinal contents was performed using the QiaAmpPowerFecal Pro DNA (Qiagen, cat. # 51804) and the V4-V5 region of 16S rRNA- genes PCR amplified using barcoded dual-index primers (520FWD-AYTGGGYDTAAAGNG and 909REV-CCGTCAATTYHTTTRAGT). Illumina compatible libraries were generated using the Qiagen QIASeq 1-step amplicon kit (Qiagen, cat. #180419 and sequencing performed on an Illumina MiSeq platform using a 2×250 Paired-End reads, generating ≥10,000 reads per sample. Data analysis was performed on the QIIME2 platform[61] and ASVs were detected using a minimum sequencing red depth of 10,000 PE reads per sample. Raw V4-V5 16S rRNA gene sequence data were demultiplexed and processed through the dada2 pipeline into Amplicon Sequence Variants (ASVs). Taxonomic assignments of ASVs up to the genus level were generated through a Naïve Bayes classifier trained on Silva database16S rRNA sequences (Silva v132) and were BLASTed against RefSeq for species-level identification with corresponding alignment statistics. Alpha diversity (Total ASVs, Shannon's index, Chao's metric, and Faith's phylogenetic diversity) and beta diversity metrics (Bray-Curtis, weighted UniFrac, and unweighted UniFrac distances) and statistical significance were calculated in QIIME2 (Mann-Whitney and PERMANOVA, n=999). Taxonomic heatmaps in Figure 1 were made using anvio v7.1.[62] Differentially abundant taxa were calculated using *MaAsLin2*.[63]

Shotgun sequencing and cross'omics with host transcriptional data

Shotgun sequencing was performed at the University of Chicago Duchossois Family Institute in the Microbiome Metagenomics Facility (DFI MMf). Raw reads were trimmed and quality filtered (Trimmomatic, v0.39)[65] and cross'assembled using megahit. Contigs <1000 bases in length were removed from the analysis, and the remaining sequences annotated for genes and functions through the KEGG database ('*anvi-gen-contigs-database*', *'anvi-run-kegg-kofams'*) and abundances of each contigs profiled into anvio v7 ('*anvi-profile*').[62] Contigs were binned with CONOCT (*'anvi-cluster-contigs'*) and manually curated to yield 87 high quality metagenome assembled genomes (MAGs) with redundancy <10% and either >90% completion or >2MB in length. MAGs were functionally assessed for the completion of KEGG metabolic modules (pathways) between JMT and FMT samples ('*anvi-compute-functional-enrichment*'). Differentially abundant MAGs containing these modules were identified using a linear discriminant analysis (LDA, LEfSe).[74] MAG abundances associated with hepatic transcriptional changes were calculated using SPARCC described by Sambhawa et al. and the coefficient plotted against the functional LDA scores to group specific MAGs to the host changes.[75]

Metabolomics

Metabolomics was performed at the University of Chicago Duchossois Family Institute in the Host-Microbe Metabolomics Facility (DFI HMMF). The metabolome of intestinal contents and plasma was analyzed across four mass spectrometry platforms to capture quantitative and qualitative levels of gut-derived metabolites with varying physiochemical properties such as hydrophobicity, size, and charge. The DFI-HMMF routinely studies intestinal and fecal material and plasma with the proposed methods and analysis pipelines. In brief, metabolites were extracted with organic solvent, dried down and resuspended for direct analyses or derivatization. Previously, all compounds have been validated by the DFI-HMMF through retention time, *m/z*, and fragmentation comparison to authentic standards and available databases. Compounds were chosen based on known host-microbe mechanisms or the compound level in fecal material was shown to significantly vary across patient populations indicating a potential role in health. Gas

chromatography-mass spectrometry (GC-MS) was used to detect 222 compounds following derivatization with pentafluorobenzyl bromide (PFBBr)[76] and trimethylsilyl-methoxamine (TMS-MOX)[77,78] in two separate reactions. SCFAs (acetate, butyrate, propionate), lactate, and succinate were quantitatively analyzed following PFB derivatization and detection by negative collision induced-gas chromatography-mass spectrometry ((-)CI-GC-MS, Agilent 8890). Another 48 PFB-derivatized compounds within the SCFA, branched chain fatty acid, amino acid, aromatic, hydroxylated fatty acid, organic acid, and indole compound subclasses were studied by normalized peak area. Positive ion electron impact-GC-MS ((+)EI-GC-MS, Agilent 7890B) was used to detect 169 molecules in the organic acid, carbohydrate, TCA intermediate, sterol, amino acid, indole and fatty acid subclasses following TMS-MOX derivatization. With the use of negative mode liquid chromatography-electrospray ionization-quadrupole time-of-flight-MS ((-)LC-ESI-QTOF-MS, Agilent 6546), 49 bile acids from the primary, secondary and glyco/tauro-conjugated subclasses were analyzed.[79] In addition to retention time validation, the standard intact and fragment masses were routinely detected with differences < 5 ppm compared to calculated values. Positive mode LC-triple quadrupole-MS ((+)LC-ESI-QQQ-MS, Agilent 6547) were used to analyze 34 indole and tryptophan catabolites. Tryptophan is an essential amino acid that is ingested in the host diet. Conversion by microbes and the host result in biologically active compounds such as serotonin, kynurenine, and melatonin. Data was analyzed by MassHunter Quantitative Analysis software (version B.10, Agilent Technologies).

RNAseq of Murine Tissues

RNA from murine jejunal mucosa, colonic mucosa, and livers (50mg) were isolated using 1mL Trizol reagent per manufacturer's instructions (ThermoFisher, cat. #15596026). Purified RNA was DNase-treated and column-purified per manufacturer's instructions (ZymoResearch, cat. #R1014). RNA quality and quantity were assessed using the Agilent bioanalyzer and strand-specific libraries prepared using the TruSEQ RNA-SEQ library protocol (Illumina) at The University of Chicago Genomics Core Facility. Library quality and quantity was assessed using the Agilent bio-analyzer and libraries sequenced on an Illumina NovaSEQ6000 or NovaSEQ-X using an Oligo-dT mRNA directional, 2x100 (Paired-End), S1 flowcell generating ~60M PE reads/sample.

Raw reads were then quality filtered (Trimmomatic, v0.39)[65] and mapped to the GRCm39 mouse genome primary assembly (GCA_000001635.9) using STAR.v2.7.10.[66] Gene counts tables were generated using '*featureCounts*' ('*subread*' v.2.0.6)[67] and normalized for batch effects between sequencing run when appropriate using '*comBat-seq*'('*sva*' in R).[68] Differential gene expression analysis was performed on the '*DESeq2*' R-package.[64] Two-way analysis for each pair of experimental groups was performed, with the DESeq2 -generated Wald statistic used to build a ranked gene list for each comparison. Pathway analysis was performed using '*fGSEA*'[69,70] with the molecular signature databases M2-Kyto Encyclopedia of Genes and Genomes (KEGG) and C5-Gene Ontology (GO) sets 'c2.cp.kegg.v7.5.1.symbols.gmt' and 'c5.all.v7.5.1.symbols.gmt' (www.gsea-msigdb.org). Custom gene sets for 'jejunal signature' and 'colonic signature' (Figure 5) were generated by filtering padj>0.05, removing genes $\log_2$FC<2, and selecting 1000 genes with the smallest padj values.

Western Blotting

Western blotting was performed according to standard procedures. Frozen murine intestinal mucosal scrapings were homogenized, passed through a 25G needle, and lysed in 2% SDS, 5% glycerol, 65mM Tris-Cl pH 7.5 containing HALT protease/phosphatase inhibitor (Thermo Scientific, cat#78441) and protease inhibitor cocktail (Roche cOmplete, SigmaAldrich, cat#4693124001). 70 ug of total protein was electrophoresed in Midi-Protean TGX gels (Bio-rad, cat#5678043) and transferred onto Immun-Blot LF-PVDF membrane (Bio-rad, cat#1620264). Blots were blocked in Everyblot blocker (Bio-rad, cat#12010020), stained with primary antibodies anti-Gata4 (Abcam, cat#ab307823) and anti-Satb2 (Abcam, cat #ab92446), probed with secondary antibodies StarBright Blue 700 anti-Rb (Bio-rad, # 12004162) and direct detection of actin using hFAB Rhodamine anti-actin (Bio-rad, #12004164) before imaging on a ChemiDoc MP Imaging System (Bio-rad, cat#12003154).

Immunohistochemistry

Immunohistochemistry was performed according to standard procedures on paraffin-embedded sections of the murine jejunum and colon. Antigen retrieval was performed for 20min in a pressure cooker with a 10 mM sodium citrate and 0.05% Tween-20 buffer (pH 6.0). Primary antibodies used were mouse anti-Gata4 (Abcam, cat#ab307823) and anti-Satb2 (Abcam, cat #ab92446). Revelation of staining was performed using ImmPRESS Polymer Reagents (Vector Laboratories, MP-7452, MP-7402) and the VOP substrate kit (Vector Laboratories,). Sections were counterstained with methyl green and imaged by the Integrated Light Microscopy Core (the University of Chicago).

Metabolic Chamber Experiments

Energy balance of mice was assessed using the Promethion High-Definition Multiplexed Respirometry System for Mice Metabolic Cage System (Sable Systems International). Mice were individually housed in metabolic cages for 5 days, with the first 48 hours of measurements discarded to account for acclimatization. Measurements were recorded in 1.5minute-3minute intervals across all cages with food and water intake recorded by gravimetric measurement. Physical movements were recorded by infrared sensor X,Y,Z-beam breaks. Oxygen consumption, carbon dioxide production, and respiratory exchange rates (RERs) were measured by indirect calorimetry and energy expenditure (kcal/h) calculated by the modified Weir equation (omitting the nitrogen term).[80] Data was recorded using IM3 software v21.0.2 and converted to XML via a custom Sable Systems macro. Data were cleaned in Python,

including identification of each diurnal cycle using environmental lux values. Within each period, the sum was calculated for beam breaks and movement, and range was calculated for food and water intake. EC_{50} was calculated for RER, VO_2, and energy expenditure[81] in R using nplr v.1-7. Analysis of covariance (ANCOVA) (body weight as covariant) was performed for each measurement between 2 groups using R.

Primary Human Jejunal Organoid Cultures

We used the protocol previously described by Sato et al., with minor adaptations.[73] Briefly, jejunum and colon biopsies (2-3 pieces) were rinsed several times in ice cold PBS to remove stool. Intestinal pieces were resuspended in 10 ml ice-cold 8 mM EDTA/PBS and agitated on a rocker at 4°C. After 30 minutes, EDTA/PBS was aspirated and replaced with 2 ml Advanced DMEM/F12 (Life Technologies,cat#11320033). Using a P1000 pipet, biopsies were triturated several times through a trimmed pipet tip to release intestinal crypts. Crypts were filtered through a 100 μm cell strainer and centrifuged at 400x*g* for 5 min at 4°C. Cells were resuspended in a 1:2 mixture of human organoid growth media (described in Sato et al.[73]) and Reduced Growth Factor Matrigel (Corning, cat#CLS356231). Matrigel droplets containing cells were plated onto 6-well plates and placed in a 37°C/5% CO_2 incubator for 1 hour until solidified. Finally, human organoid growth media[73] was added to the culture. Organoids were cultured for at least 3-4 weeks, with media changes twice per week and passaging and expansion every 2 weeks.

On the evening prior to stimulation, organoid growth media was exchanged for basal media (Advanced DMEM/F12, 1X N2, 1X B27, 1.25 mM N-acetyl-cysteine, and 10 mM Nicotinamide). During the next morning, luminal aspirates were thawed, spun 5min at 500x*g*, and 0.22 μm sterile-filtered (Millipore, PVDF-membrane, cat. #SCGP205RE). Luminal aspirate from either jejunum or colon were added to organoids for a final concentration of 10% (v/v). Organoids were stimulated for 24h hours, then collected. Cells and Matrigel were centrifuged at 400xg for 5 min at 4°C. Media and Matrigel were removed and cell pellet was resuspended in 1 ml Trizol (ThermoFisher, cat. #15596026). Total RNA was isolated per manufacturer's instructions and DNase-treated/column-purified per manufacturer's instructions (ZymoResearch, cat. #R1014). RNAseq was performed and analyzed in the same manner as the murine tissues detailed under 'RNAseq of Murine Tissues'.

QUANTIFICATION AND STATISTICAL ANALYSIS

For all endpoint measurements unless otherwise noted, a one-way ANOVA was performed followed by Tukey's multiple comparisons test, $p < 0.05$, using GraphPad Prism v10. Heatmaps were generated in orange v.3.2 or '*seaborn*'[71] in python and modified in Inkscape v1.3.2.

Supplemental figures

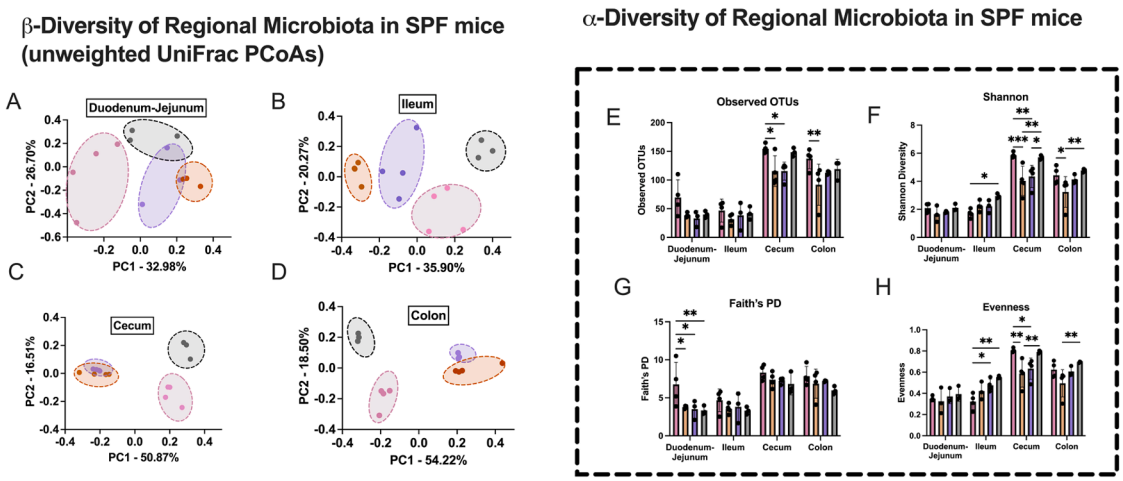

Figure S1. Region-specific diversity in post-ABX mice 1 month after MT, related to Figure 1

(A–D) rRNA sequencing was performed on the intestinal contents 1 month after MT. β-diversity was assessed by principal coordinate analysis (PCoA) of the unweighted UniFrac distance matrix for each intestinal region (colored by treatment group, PBS-gray, JMT-pink, CMT-orange, FMT-lavender) demonstrates unique microbial compositions after MT in the duodenum-jejunum (A), ileum (B), cecum (C), and colon (D). All pairwise comparisons are significant between treatment groups (PERMANOVA, pairwise $^*p < 0.05$).

(E–H) α-Diversity between treatment groups was assessed for each intestinal region by calculating observed OTUs (E), Shannon's diversity (F), Faith's phylogenetic diversity (G), and evenness (H) (2-way ANOVA, post hoc Tukey's, $^*p < 0.05$).

All error bars represent ± SD.

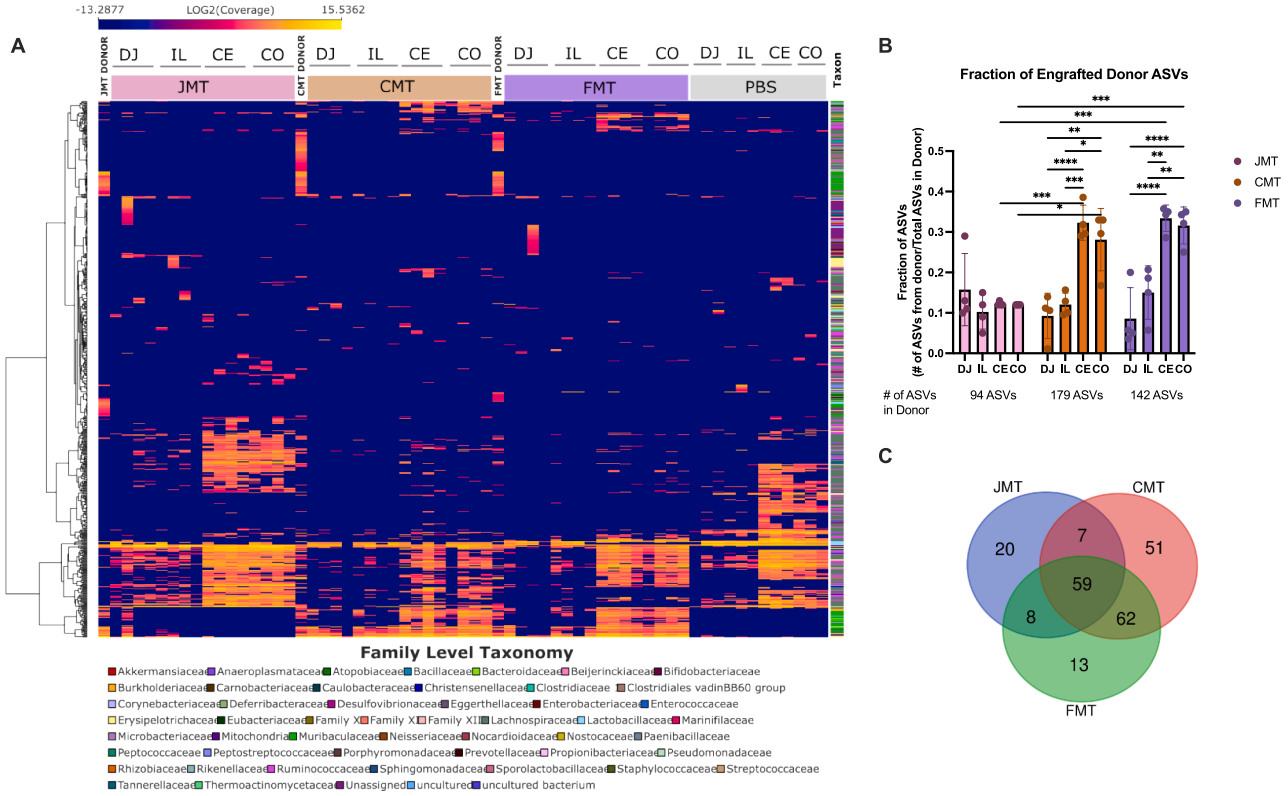

Figure S2. ASV-specific tracking across recipients, related to Figure 1

(A) 16S rRNA sequencing of intestinal contents 1 month after MT. ASVs were tracked from the donor material provided to the recipient mice, examining specific ASVs across the bowel (DJ, duodenum-jejunum; IL, ileum; CE, cecum; and CO, colon).

(B) Fraction of ASVs from the specific donor that engrafted show that ~10%–30% of donor ASVs engraft (2-way ANOVA, post hoc Tukey's, $*p < 0.05$).

(C) These ASVs represent both unique and shared ASVs across the 3 donor materials (JMT, CMT, or FMT).

All error bars represent ± SD.

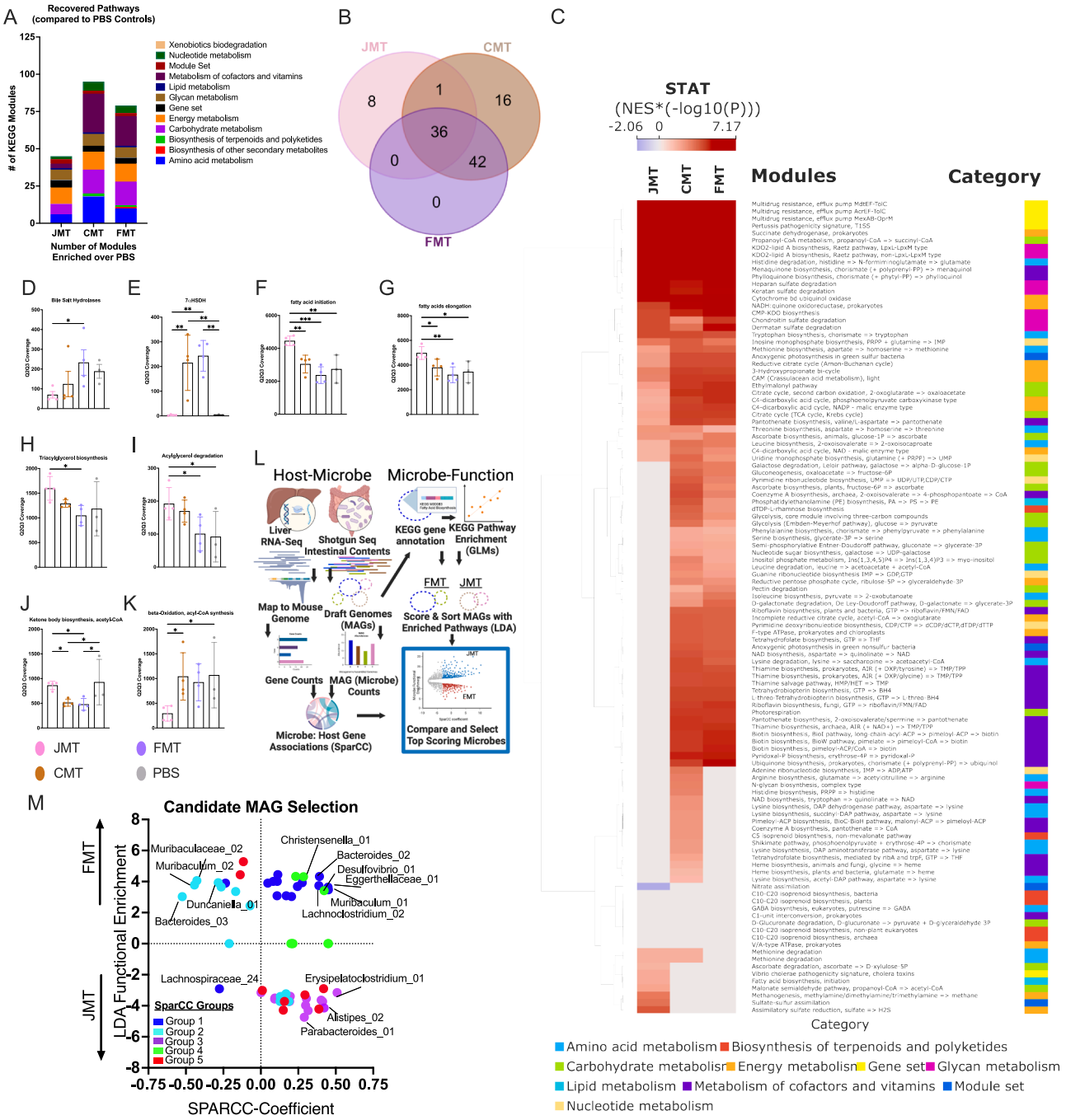

Figure S3. Shotgun metagenomic sequencing reveals differences in functional potential, related to Figures 1 and 4

(A) Shotgun sequencing of the colonic contents 1 month post MT. KEGG-based gene coverages of resulting microbiomes reveals CMT and FMT recover a greater number of pathways than JMT (relative to PBS, no MT).

(B) Overlap of recovered functional modules reveals that any MT recovers a significant number of functional pathways (36), but that FMT and CMT recover a unique 42 pathways not recovered by JMT in the colon.

(C) Significant pathways recovered over PBS for each MT are shown as the normalized enrichment score (NES)* [$-\log_{10}(P \text{ value})$] and shown as a heatmap.

(D–K) Gene coverages for KEGG orthologs (KOs) mapping to bile acid genes and lipid pathways reveal JMT to be low in bile salt hydrolases and 7α-HSDHs, high in fat productions genes, and low in genes for beta-oxidation.

(L) Cross-omics identification of strains associated with liver transcriptional changes were identified using a cross-omics pipeline. Differentially enriched functions between JMT and FMT using generalized linear models (GLMs) and differentially abundant strains containing those functions (linear discriminant analysis, LDA).

(legend continued on next page)

(M) Abundances of reconstructed metagenome-assembled genomes (MAGs) were then associated with liver transcriptome changes using SPARCC and the two values plotted to identify MAGs containing specific functions and associated with host transcriptional changes and likely to drive the changes observed. All error bars represent ± SD.

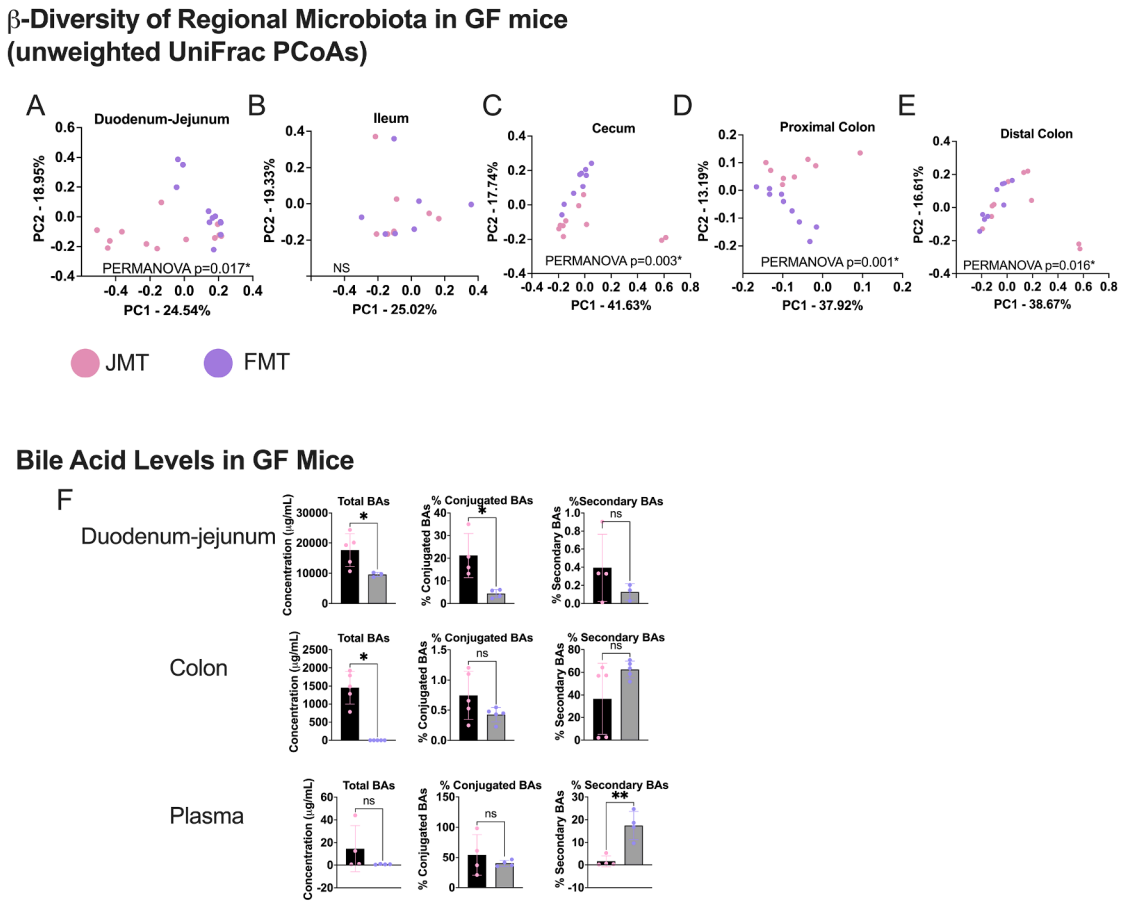

Figure S4. Regional diversity and bile acid profiles in GF mice, related to Figure 3

(A–E) β-Diversity of each intestinal region in GF mice 1 month after MT was assessed by principal coordinate analysis (PCoA) of the unweighted UniFrac distances for the duodenum-jejunum (A), ileum (B), cecum (C), proximal colon (D), and distal colon (E). All pairwise comparisons were significant, except in the ileum (PERMANOVA, *$p < 0.01$, JMT-pink, FMT-lavender).

(F) Total bile acid levels, % conjugated bile acids, and % secondary bile acids from the duodenum-jejunum, colon, and plasma were assessed by mass spectrometry (Student's t test, *$p < 0.05$).

(G–I) Concentrations of the 15 most abundant bile acids are shown for the duodenum-jejunum (G), colon (H), and plasma (I) (one-way ANOVA, post hoc Tukey's, *$p < 0.05$).

All error bars represent ± SD.

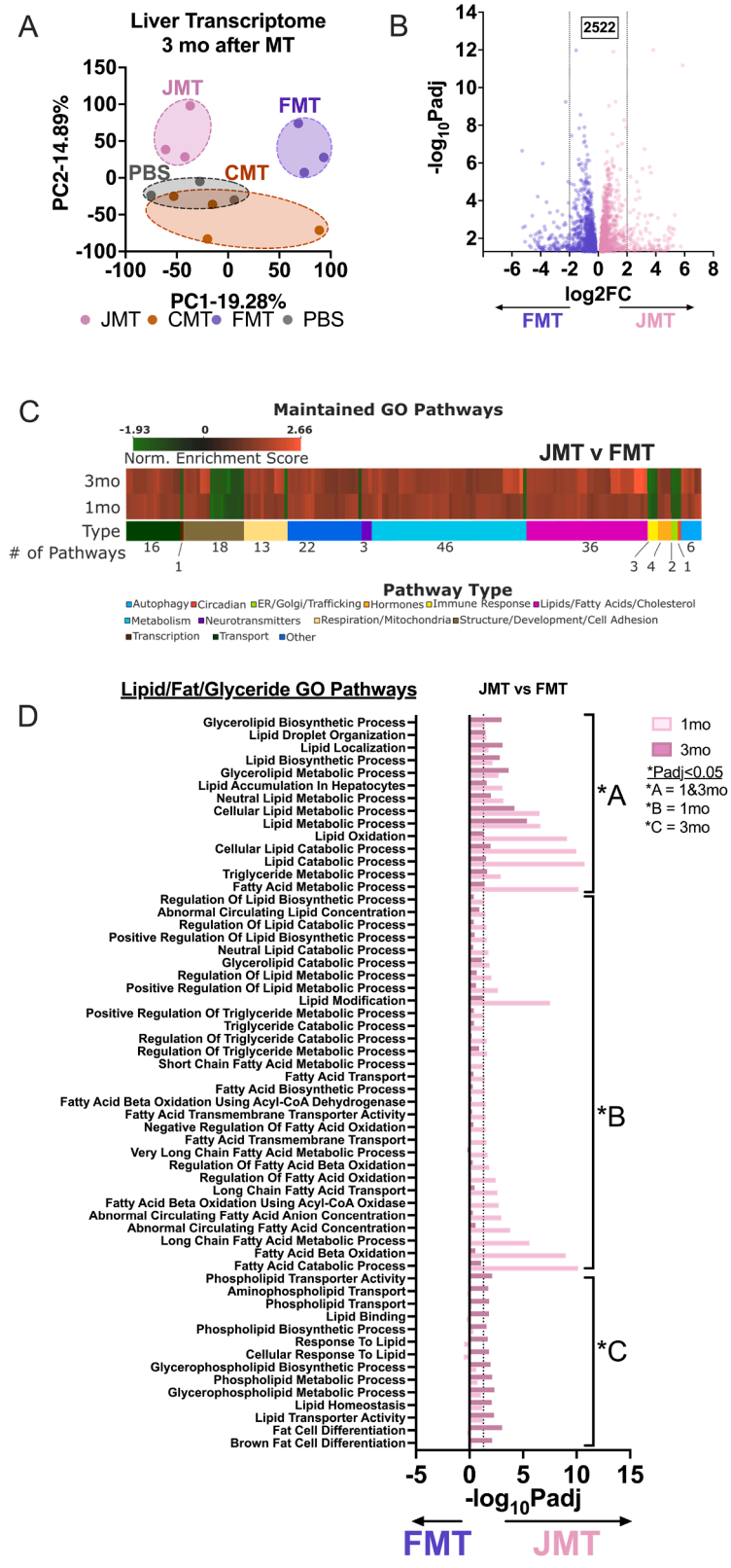

(legend on next page)

Figure S5. Hepatic transcriptomes remain altered at 3 months and persist in altered metabolic and lipid pathways, related to Figure 4

(A) Hepatic transcriptomes were assessed 3 months after MT. Principal coordinate analysis of the hepatic transcriptomes demonstrate significant differences between JMT and FMT (PC1 = 19.28%, PERMANOVA, $*p < 0.01$) (PBS, gray; JMT, pink; CMT, orange; FMT, lavender).

(B) Differential gene expression between JMT and FMT revealed 2,522 DEGs (*DESeq2*, $*p\text{adj} < 0.05$).

(C) Maintained GO (Gene Ontology) pathways between 1 and 3 months were assessed between JMT and FMT. All significant pathways between 1 and 3 months are categorized and show that many lipid and metabolic pathways are maintained after 3 months (*fGSEA*, $*P\text{adj} < 0.05$). Comparisons of lipid, fat, and glyceride GO pathways between FMT and JMT ($-\log10P\text{adj}$). Pathways significant for both 1 and 3 months (*A), 1 month only (*B), and 3 months only (*C) are noted.

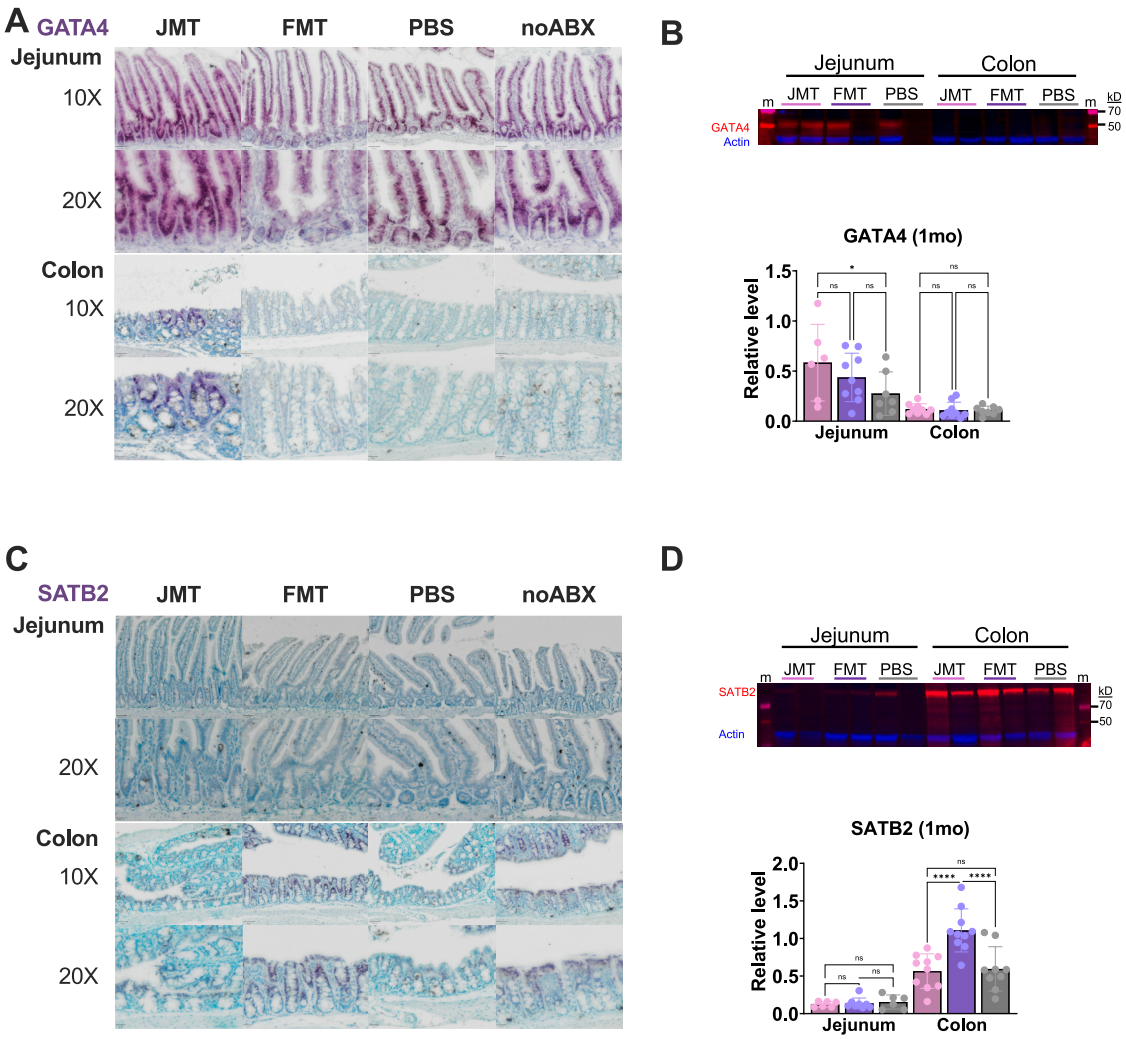

Figure S6. Functional expression of key transcription factors involved in tissue identity, related to Figure 5

(A) IHC of jejunum and colon reveals enhancement of jejunum Gata4 nuclear staining after JMT loss of nuclear staining in FMT relative to normal animals 1 month after MT. Patches of Gata4 can be found in the colon after JMT.

(B) Expression of Gata4 with WB reveals enhancement of Gata4 after JMT in the jejunum.

(C) Increased numbers of Satb2+ cells could be identified in the colon after FMT and fewer after JMT, but no difference detected in the jejunum.

(D) Quantification of Satb2 protein levels by WB revealed increased Satb2 after FMT in the colon. Immunohistochemistry (IHC) of Swiss rolls are representative images of $n = 3$ mice/group. Statistical significance of Gata4 and Satb2 in jejunal and colonic mucosal scrapings ($n = 6–9$/group) was calculated using an ANOVA with post hoc Tukey's ($^*p < 0.05$).

All error bars represent ± SD.